

SOUTHERN CALIFORNIA PARTICLE SUPERSITE

Progress Report for Period March 15, 2002 – July 1, 2002

United States Environmental Protection Agency

Principal Investigator: John R. Froines, Ph.D., UCLA School of Public Health

Co-Principal Investigator: Constantinos Sioutas, Sc.D., USC School of Engineering

1. Introduction

The overall objective of the Southern California Particle Supersite is to conduct research and monitoring that contributes to a better understanding of the measurement, sources, size distribution, chemical composition and physical state, spatial and temporal variability, and health effects of suspended particulate matter (PM) in the Los Angeles Basin (LAB). This report addresses the period from March 1, 2002 through June 1, 2002. It is divided into 8 sections, each addressing a specific research area, including an update on our Data Management report. Furthermore, a major portion of the information included in this report has been either submitted or accepted for publication in peer-reviewed journals. Below is a list of manuscripts either submitted or accepted for publication which were produced through the Southern California Supersite funds and in which the EPA Supersite program has been acknowledged.

Publications

Singh, M., Jaques, P. and Sioutas, C. "Particle-bound metals in source and receptor sites of the Los Angeles Basin". *Atmospheric Environment*, 36(10): 1675-168, 2002 .

Kim, S., Shi, S., Zhu, Y., Hinds, W.C., and Sioutas, C. "Size Distribution, Diurnal and Seasonal Trends of Ultrafine Particles in Source and Receptor Sites of the Los Angeles Basin". *Journal of Air and Waste Management Association*, 52:174-185, 2002

Li, N., Kim, S., Wang, M., Froines, J.R., Sioutas, C. and Nel, A. "Use of a Stratified Oxidative Stress Model to Study the Biological Effects of Ambient Concentrated and Diesel Exhaust Particulate Matter". *Inhalation Toxicology*, 14(5): 459-486, 2002

Zhu, Y., Hinds, W.C., Kim, S., Shen, S. and Sioutas, C. "Study on Ultrafine Particles and other Vehicular Pollutants near a Busy Highway Dominated by Diesel Traffic". *Atmospheric Environment*. Submitted, March 2002

Eiguren, A, Miguel, A.H, Jaques, P. and Sioutas, C. "Evaluation of a Denuder-MOUDI-PUF Sampling System to Determine the Size Distribution of Semivolatile Polycyclic Aromatic

Hydrocarbons in the Atmosphere”. Manuscript accepted for publication in *Aerosol Science and Technology*, June 2002.

Zhu, Y., Hinds, W.C., Kim, S and Sioutas, C. “Concentration and Size Distribution of Ultrafine Particles near a Major Highway”. *Journal of Air and Waste Management Association*, accepted for publication, September, 2001

Geller, M.D., Kim, S. Misra, C., Sioutas, C., Olson, B.A and Marple, V.A. “Methodology for measuring size-dependent chemical composition of ultrafine particles “ *Aerosol Science and Technology*, 36(6): 748-763, 2002

Misra, C., Kim S., Shen S. and Sioutas C. “Design and evaluation of a high-flow rate, very low pressure drop impactor for separation and collection of fine from ultrafine particles”. *Journal of Aerosol Science*, 33(5): 735-752, 2002 -Fine, P.M., Hering, S.V., Jaques P.A. and Sioutas, C. “Performance Evaluation and Field Use of a Continuous Monitor for Measuring Size-Segregated PM_{2.5} Particulate Nitrate”. Manuscript submitted to *Aerosol Science and Technology*, March 2002

Misra, C., Geller, M.D., Solomon, P.A. and Sioutas, C. “Development of a PM₁₀ Inertial Impactor for Coarse Particle Measurement and Speciation.” Submitted to *Aerosol Science and Technology*, April 2002

Stolzenburg, M.R., Dutcher, D., Kirby, B., Kreisberg, N. and Hering, S.V. (2002). Automated Measurement of the Size Distribution of Airborne Particulate Nitrate. Submitted to *Aerosol Science & Technology*, April 002

Shen, S., Zhu, Y., Jaques PA and Sioutas C. “Evaluation of the SMPS-APS system as a Continuous Monitor for PM_{2.5} and PM₁₀”. *Atmospheric Environment*, in press , 2002

2. PIU Sampling Location and Status

A key feature of our Supersite activities has been in the ability to conduct state-of-the-art measurements of the physicochemical characteristic of PM in different locations of the Los Angeles Basin (LAB). We originally proposed a 2.5-year repeating cycle of measurements at five locations. Each location will be sampled during a period of intense photo-chemistry (defined approximately as May – October) and low photochemical activity (defined as the period between November – April). During the period of this progress report, PM sampling with the Particle Instrumentation Unit (PIU) continued at Claremont, our fourth sampling site. We have completed all chemical speciation analysis for integrated samples collected in Claremont from September 2001 through this May 2002. We have continued to make size-segregated on-line measurements of particulate nitrate and carbon using the Integrated Collection and Vaporization System (ICVS) developed by Aerosol Dynamics Inc. Two continuous BAM monitors have been installed and will be paired with the USC-TEOM coarse monitor to generate hourly data of coarse, fine and ultrafine PM. Additionally, we have continued to make our mobile particle trailer available for co-located exposure studies at Claremont, and the future location at USC.

The trailer is scheduled to remain at Claremont for the remainder of the summer, and will be relocated to the fifth site on USC campus towards the end of August 2002. USC campus is about 1-2 miles upwind of two major freeways, and about 3-5 miles south of downtown Los Angeles.

The following health studies have been supported by the Supersite measurements: In vitro studies undertaken by Drs. Andre Nel and Arthur Cho (UCLA) investigating the hypotheses that organic constituents associated with PM, including quinones, other organic compounds (PAHs, nitro-PAHs, and aldehydes/ketones) and metals, are capable of generating reactive oxygen species (ROS) and acting as electrophilic agents. These are ongoing studies. Animal inhalation toxicology studies using Concentrated Ambient Particulates (CAP) investigating the hypotheses that atmospheric chemistry is important in the toxicity of PM and co-pollutants, airway injury and cardiovascular effects will be greater at receptor sites downwind of source sites along the mobile source trajectory in the Los Angeles basin. Led by Drs. Harkema (University of Michigan), Kleinman (UC Irvine), Froines and Nel (UCLA), these co-located studies that commenced during the summer season in Claremont have continued through this past Winter to investigate seasonal changes in toxicity.

3. Time Integrated Size Fractioned Chemical Speciation for Claremont

Introduction

Our current sampling scheme continues to involve the use of three MOUDIs for 24-hour averages: size-fractionated measurements of ambient and concentrated PM mass and chemical composition. Sampling is conducted once a week, on a Tuesday, Wednesday or Thursday, in order to coincide with one of the sampling days of the AQMD speciation network (which takes place every 3rd day). However, this schedule is flexible to be adjusted for our “intensive” particulate characterization studies and/or for our support of co-located health effects exposure studies. Typically, ambient data are averaged over 24 hours (midnight to midnight), whereas for exposure or source contribution measurements, the time integrals may vary. In each run, consistent with our original Supersite proposal, we have used three collocated Micro-Orifice Uniform Deposit Impactors (MOUDI) to generate five PM size ranges:

<0.1 μm	(ultrafine particles)
0.1- 0.32 μm	(accumulation mode, “condensation” sub-mode)
0.32 – 1.0 μm	(accumulation mode, “droplet” sub-mode)
1.0 – 2.5	(“intermediate” mode)
2.5-10 μm	(coarse particles)

In addition to mass concentration, the following chemical components have been analyzed within these size groups: inorganic ions (i.e., sulfate, nitrate, ammonium), analyzed by ion chromatography (Dionex); trace elements and metals, analyzed by XRF; and the elemental and organic carbon (EC/OC) content is analyzed by thermal optical detection.

Results

Figure 1 presents the size distribution of particle mass measured by the MOUDI for PM less than 2.5 μm , and by the Partisol for the coarse mode. Fine PM (18.9 $\mu\text{g}/\text{M}^3$) is slightly greater than Coarse (16.3 $\mu\text{g}/\text{m}^3$). In the Fine fraction, mass predominates in the accumulation “droplet” sub-mode (8.8 $\mu\text{g}/\text{m}^3$), suggesting aged particles. the Ultrafine mode consists of the lowest mass at 1.1 $\mu\text{g}/\text{m}^3$. PM_{2.5} mass measured by the MOUDI and integrated PM_{2.5} mass measured by the continuous SMPS-APS system (see previous report, and Shen, et al., 2002) are compared to that of the Partisol (Figure 2). Both the MOUDI and SMPS-APS mass is highly correlated to that of the Partisol: R-sq = 0.84, and 0.78, respectfully - both with slopes close to 1:1. The SMPS is about 10% lower than the Partisol, though.

Size speciated mass measurements are presented in Figures 3 - 6. Figure 1 and 2 show that the coarse fraction is dominated by Metal Oxides, likely from local re-suspended road dust. The Fine fraction is dominated by Ammonium Nitrate, which predominates in the droplet (3.6 $\mu\text{g}/\text{m}^3$), and secondly in the intermediate mode (2.7 $\mu\text{g}/\text{m}^3$). Claremont is a receptor site North West of the dairy farms, and diurnally receives winds from this direction, likely contributing to the relatively high Ammonium Nitrate in the larger modes of the fine PM fraction. Organic Carbon is higher in PM_{2.5} than coarse, and highest in the Accumulation Mode (3.3 $\mu\text{g}/\text{m}^3$). It is in greatest relative concentration in the droplet mode (1.8 $\mu\text{g}/\text{m}^3$). Since Claremont is a "freeway" trajectory site, it may be expected that aged enlarged OC-associated particulate matter predominate. Of the Accumulation modes, Ammonium Nitrate is greatest in the droplet mode, while Organic Carbon in the condensation mode.

Figure 5 presents a comparison of the size speciated total filter mass to that of the summed chemical species described above. Figure 6 presents a ratio of the two by size fraction. Except for the Ultrafine mode (0.66) and Coarse mode (1.4), the sum of the measured chemical groups explains between 80 to 90% of the total measured particulate mass for the other modes. Since the ultrafine filter mass is less than 5% of the total filter mass, the relative chemical mass is not as reliable a measurement.

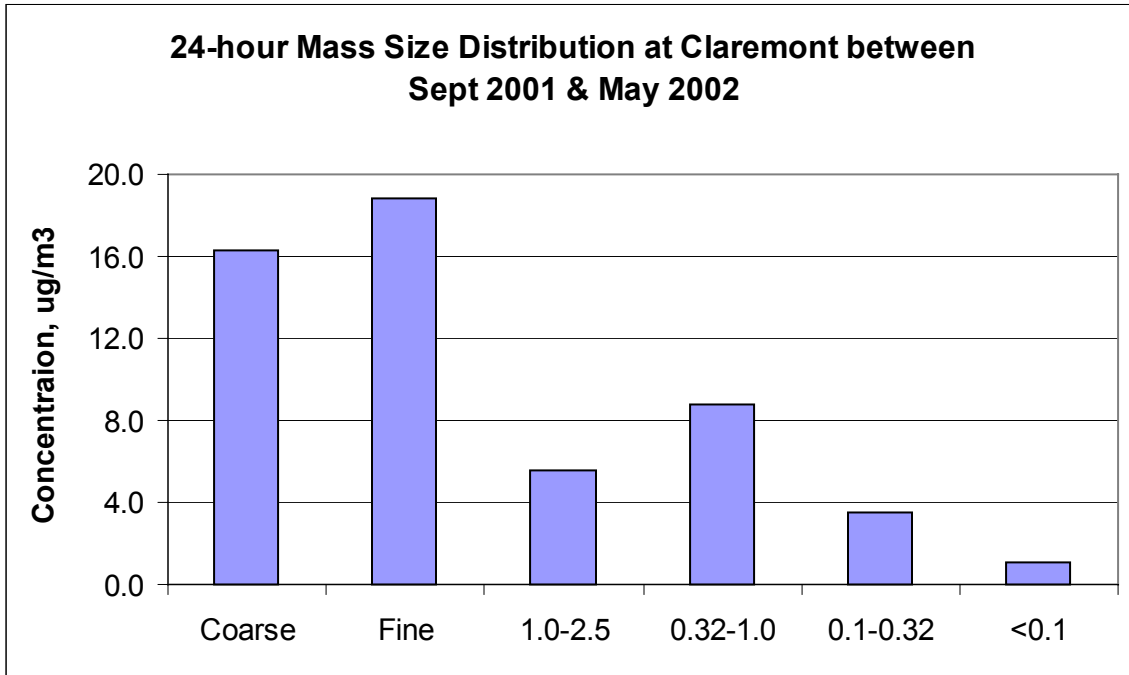


Figure 1. Size distribution of particle mass measured by MOUDI (< 2.5 um) and Partisol (10 - 2.5 um).

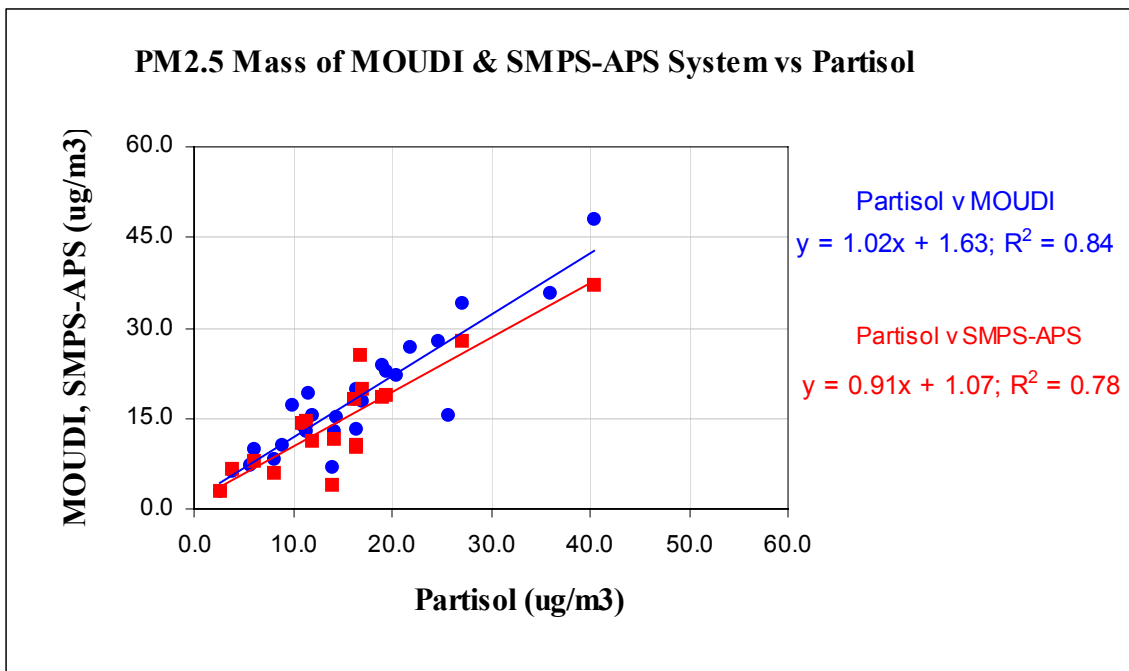


Figure 2. Comparison of PM2.5 by MOUDI and SMPS-APS mass to that of the Partisol.

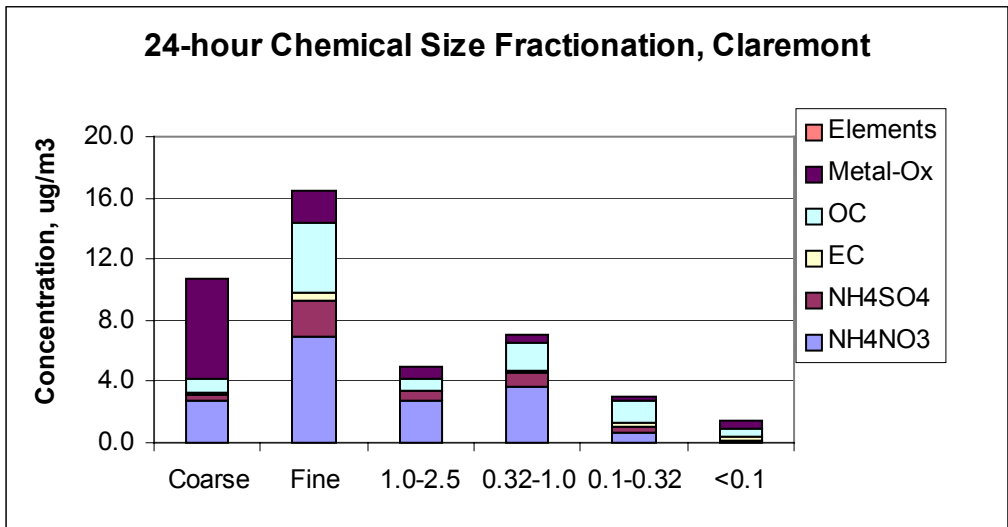


Figure 3. Chemical size speciation of 6 chemical groups.

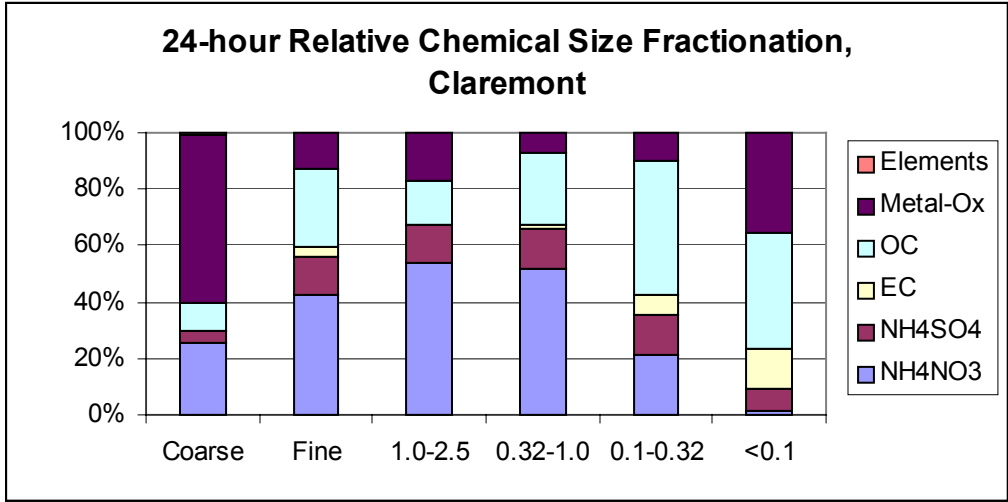


Figure 4. Relative chemical size speciation of 6 chemical groups.

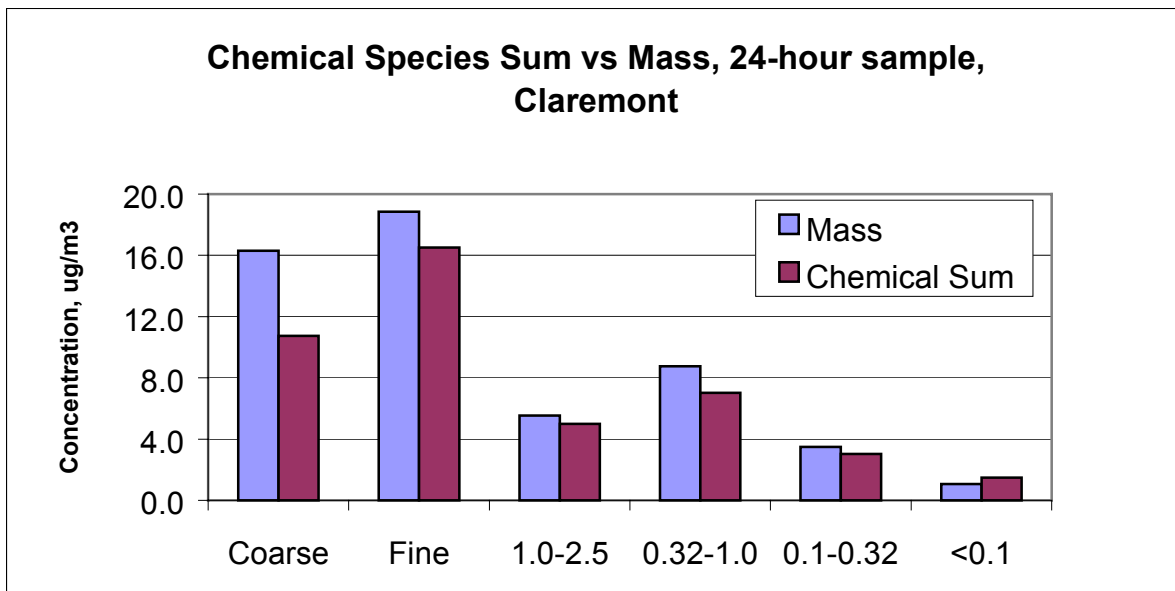


Figure 5. Comparison of Size speciated mass to the sum of all measured compounds.

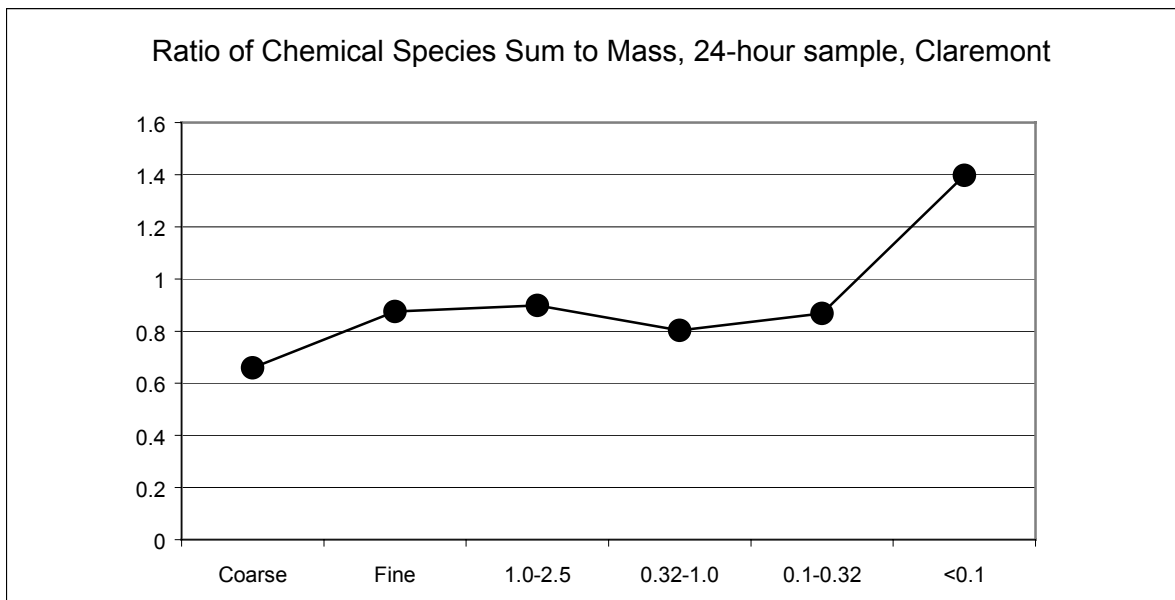


Figure 6. Ratio of the sum of all measured compounds to total mass, by size fraction.

4. Seasonal Trends of Ultrafine Particles near Freeways

It is now well established that increases in the concentration of fine particulate matter in urban areas are associated with increases in morbidity and mortality. It is not known what properties of fine particulate matter cause these effects, but one candidate is ultrafine particles. These are particles less than 100 nm or 0.1 μm in size and are found near combustion sources, such as motor vehicles. Previously we conducted systematic ultrafine particle studies near two freeways in the Los Angeles basin, Interstate 405 and 710 in summer with moderately high temperature and humidity in Los Angeles basin (Zhu et al., 2002 a, b). The average temperature during this sampling period was 30°C and the average relative humidity was 66 %. Measurements at both freeways showed rapid decrease in particle number concentration and a significant changes in particle size distribution with increasing distance downwind from the freeway for particles in the size range of 6 nm to 220 nm. Strong seasonal changes have been reported for the concentration and size distribution of ultrafine particles. Warmer temperature in Los Angeles Basin are characterized by higher temperature differences between the coastal regions and inland valleys, thus creating a higher temperature inversion aloft and a stronger onshore flow. In general, the concentration of particles in vehicle exhaust in the nuclei mode increases by nearly one order of magnitude, as the temperature is reduced from 25°C to 15°C (Kittelson, 1998). The focus of the present study is to evaluate ultrafine particles in the vicinity of freeways under winter conditions in the Los Angeles Basin, to compare these results with those determined in summer, and to investigate the degree to which differences in meteorological conditions, such as temperature, humidity and atmospheric mixing depth affect the characteristics of ultrafine particles.

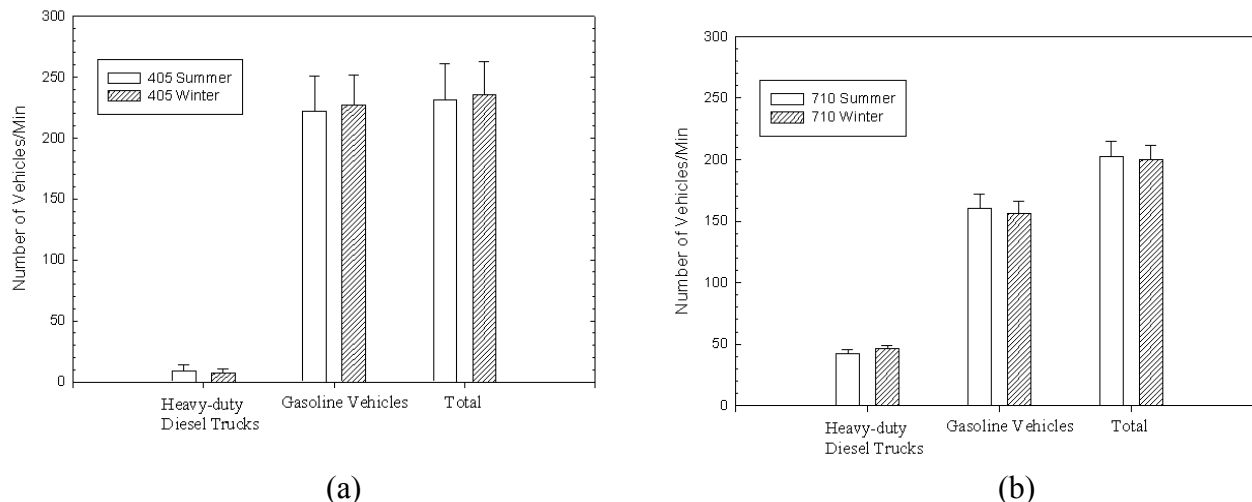


Figure 1. Traffic volume comparison in summer and winter for the (a) 405 and (b) 710 freeways. Bars indicate one standard deviation.

Figures 1a-b compare the traffic volume in summer and winter on the 405 and 710 freeways, respectively. Freeway 405 passes through West Los Angeles and is considered one of the busiest freeways in the United States with more than 95% of traffic being gasoline-powered vehicles (Zhu et al., 2002a). The average traffic volume per hour during the winter sampling period on the 405 freeway was: 13,100 cars, 360 light trucks, 540 heavy-duty trucks, and 14,000 total vehicles. These values are not statistically different from those reported by Zhu et al. (2002a) in summer. Freeway 710, passing through the City of Downey, is considered a major truck shipping route in Southern California with about 25-30% of traffic being heavy-duty diesel trucks (Zhu et al., 2002b). The average traffic volume per hour during the winter sampling period on the 710 freeway was: 8,450 cars, 840 light trucks, 2,780 heavy-duty trucks, and 12,000 total vehicles. These values are not statistically different from those reported by Zhu et al. (2002b) in summer near the 710 freeway.

Table 1. Comparison of sampling conditions in summer and winter

	Summer	Winter
Temperature (Celsius)	30.3±3.7 ^a	23.2±4.0
Relative Humidity (%)	66.4±14.8	43.1±21.4
Wind Speed (m/s)	1.36±0.66	1.27±0.67
Traffic Density on 405 Freeway (vehicles/min) ^b	231±30	236±27
Traffic Density on 710 Freeway (vehicles/min) ^b	203±12	200±11
Solar Zenith Angles (deg) [*]	25.1±6.3	64.4±1.4
Control CPC reading near 405 ($\times 10^{-5}/\text{cm}^3$)	1.16±0.87	1.40±1.09
Control CPC reading near 710 ($\times 10^{-5}/\text{cm}^3$)	1.22±1.11	1.49±1.12

* Finlayson-Pitts and Pitts, Chemistry of the Upper and Lower Atmosphere, 2000 Academic Press. Table 3.9.

a. Mean \pm one standard deviation.

b. Both directions combined.

Table 1 summarizes the mean and standard deviation for meteorological sampling conditions, total vehicles, and control CPC readings in summer and winter. Since the raw data did not meet the normality criteria for a t-test, the non-parametric Mann-Whitney rank sum test was used to compare two independent groups of sampled data in summer and winter. Test results show that the traffic density near the 405 and 710 freeways are not statistically different in summer and in winter, while temperature, relative humidity, wind speed, solar zenith angle and CPC readings are all significantly different with a P value less than 0.001.

Figures 2a-b show the ultrafine particle size distribution at different sampling locations near the 405 freeway in summer and winter, respectively. As shown in Figure 2a, three distinct modes were observed during the summer season, 30-m downwind from the freeway. The smallest mode, around 13 nm, shifted to a larger geometric mean diameter, 16 μm , and the modal number concentration dropped to one third of the maximum at 60 m downwind.

Figure 2b illustrates a different situation in the winter season. Only one dominant particle mode was observed for all sampling locations. At 30 m downwind from the 405 freeway, this mode occurred around 7 nm, rather than 13 nm, with a modal number concentration of $1.8 \times 10^5 / \text{cm}^3$. This mode also persisted at distances up to 300m downwind of the freeway and did not shift to larger size range. Furthermore, although the modal concentration decreased significantly with increasing distance, it did not drop as fast as it did in summer. While this mode was not observed at downwind distances greater than 60 m in summer, it was observed at all sampling locations in winter. It is also of particular note that unlike summer ultrafine particle concentrations measured at 300 m downwind of the 405 freeway were still distinguishable from background measurement in winter.

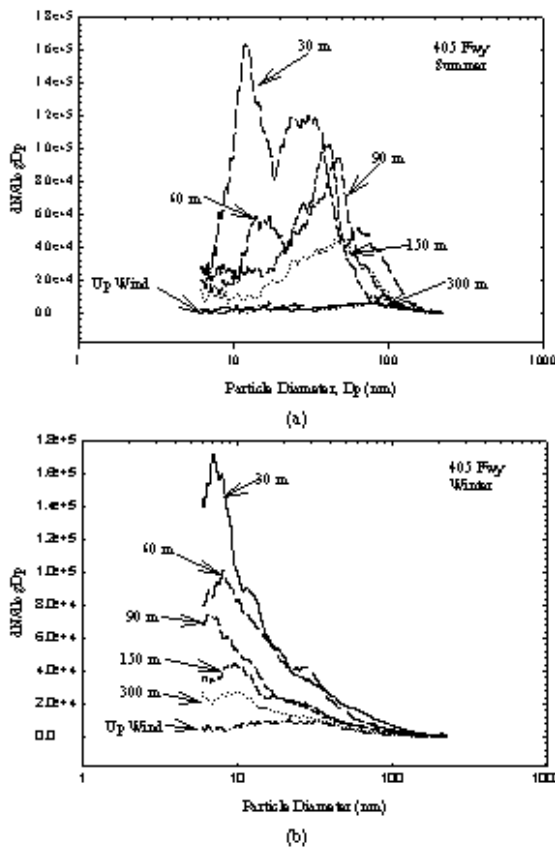


Figure 2. Ultrafine particle size distribution near the 405 freeway in (a) summer and (b) winter.

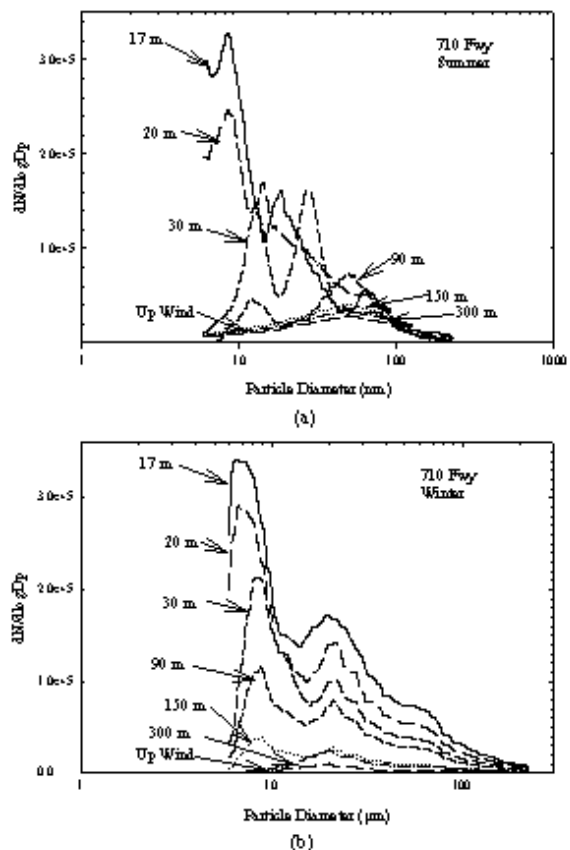


Figure 3. Ultrafine particle size distribution near the near the 710 freeway in (a) summer and (b) winter.

Figures 3a-b were prepared in the same way as Figures 2a-b, showing the ultrafine particle size distribution at different sampling locations near the 710 freeway in summer and winter, respectively. For the predominant mode (diameter < 10 nm), similar trends were observed. This mode shifted to a larger size range and disappeared after 90 m from the 710 freeway in summer. By comparison, in wintertime, this mode persisted up to 150 m downwind from the freeway. The decay in modal concentration with distance from the freeway was slower than that observed during the summer experiments. Contrary to what was observed near the 405 freeway, a second mode around 20 to 30 nm existed in winter near the 710 freeway. This is presumed to be due to the much higher diesel emissions on the 710 freeway. Similar to the predominant mode, the second mode remained around 20 to 30 nm for all sampling locations and did not shift to larger size ranges significantly. Its modal concentration decreased more slowly in winter than in summer.

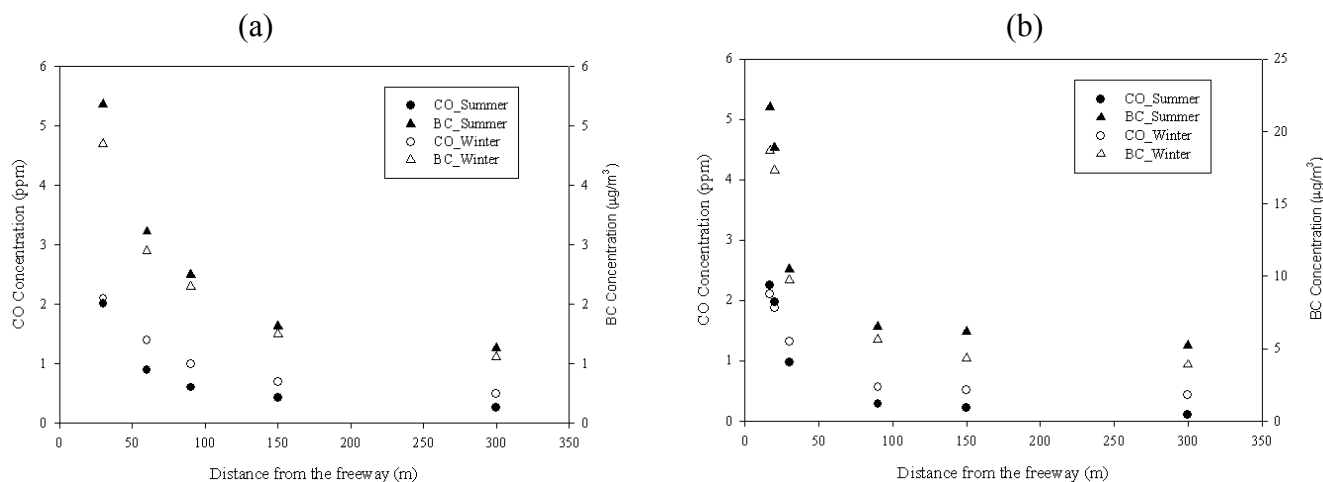


Figure 4. Comparison of Carbon Monoxide (CO) and Black Carbon (BC) concentration decay in summer and winter near (a) the 405 freeway and (b) the 710 freeway.

Figures 4a-b compare the concentration of carbon monoxide (CO) and black carbon (BC) in summer and winter with increasing distance from freeways 405 and 710, respectively. The decay rates for these two pollutants are slightly greater in summer than in winter for both freeways, which suggests that atmospheric dilution effect is stronger in summer, possibly because of the increased mixing depth of the atmosphere during that period. An additional factor for the lower decay rates in the winter may be the lower wind speeds during that period. According to classic Gaussian dispersion models, the pollutant's concentration is inversely proportional to wind speed at a given downwind distance from the emission source. Since the average wind speed in winter is about 93% of that in summer, the dilution effect may be about 7% weaker in winter assuming all other influencing factors are the same.

References:

Kittelson, D.B., 1998. Engines and Nanoparticles: A Review. *Journal of Aerosol Science* 29, 575-588.

Zhu Y., Hinds, W.C., Kim, S., Sioutas, C., 2002a. Concentration and Size Distribution of Ultrafine Particles near a Major Highway. Accepted for Publication in *Journal of Air and Waste Management Assoc.*

Zhu Y., Hinds, W.C., Kim, S., Shen, S., Sioutas, C., 2002b. Study of Ultrafine Particles near a Major Highway with Heavy-duty Diesel Traffic. Accepted for Publication in *Atmospheric Environment*.

5. Reactive Organic data

During the reporting period, the SCPCS Chemical Analysis Laboratory (SCPCS-CAL) performed detailed quantification of gas- and particle-phase chemical species in ambient air, vehicular emissions, and concentrator samples generated by SCPCS investigators.

A summary of findings and conclusions is presented for the study of PAHs, quinones, and carbonyls in the CHS Sites of Atascadero, San Dimas, Riverside, Lompoc, Mira Loma, and Upland.

Summary

The major objective of this component of the study is to assess the inter-community variability of ambient levels of polycyclic aromatic hydrocarbons (PAHs), quinones, and carbonyls in the Southern California communities participating in the California Air Resources Board CARB-sponsored CHS. It is a longitudinal respiratory health study of several thousand Southern California school children, designed to investigate possible association between chronic respiratory health outcomes and ambient air pollutant concentrations. Samplers are rotated between two sets of CHS sites every three months, in order to assess seasonal variability at the sites and to provide sufficient information to determine annual levels of the respective pollutants at each sampling location. With this approach, seasonal information can be developed for six CHS sites per year, and all 12 communities will be characterized over a two-year field operations period.

Included in this report are the results for:

Cycles 1 (early summer) and 3 (autumn): Atascadero, San Dimas, and Riverside
Cycle 2 (late summer): Lompoc, Upland and Mira Loma.

Target analytes and respective codes are listed in Tables 1 and 2, Appendix A.

PAH Results

The particle-phase ($PM_{2.5}$), vapor-phase, and total PAH (particle+vapor phase) concentration means for the target PAHs for cycles, 1, 2, and 3 are shown in figures 1-4.

For Atascadero, San Dimas and Riverside, compared with the early summer period, mean particle-phase concentrations of the less volatile PAHs (PYR to IND) were significantly higher in the autumn (figures 1A-C). At all 3 sites, BGP had the highest mean concentrations during the two periods. It is note worthy that the particle-phase concentrations during the autumn did not vary much among the 3 sites.

For cycle 1 sites, the vapor-phase PAH concentrations were also generally higher in the autumn, especially for the more volatile PAHs (figures 2A-C). For all samples, the concentration of naphthalene was an order of magnitude or higher than that of other semivolatile target PAHs (Figures 2A-C).

The mean total PAH (particle+vapor phase) concentrations are shown in figures 3A-C. Total PAH concentration is the most accurate measurement of atmospheric PAHs, as it is not affected by sampling artifacts known to occur when sampling with filters. The increased PAH concentrations during the autumn may reflect lower prevailing ambient temperatures, with attending lower atmospheric inversion heights, less mixing, and decreased atmospheric reactivity. Average temperatures during the sampling periods were: 75.5 °F during the early summer (cycle 1), 66.6 °F during the late summer (cycle 2), and 58.9 °F during the autumn (cycle 3).

Mean particle-phase (PM_{2.5}), vapor-phase and total PAH concentrations measured in later summer (cycle 2) in Lompoc, Upland and Mira Loma are shown, respectively, in figures 4A-C. Consistent with vehicular traffic, except for NAP and FLU in PM_{2.5} in Lompoc (figure 4A), the concentrations were much higher at the urban sites, with Mira Loma showing the highest levels. The mean concentrations found at these sites during late summer are also generally lower than the levels measured during the autumn at the other 3 sites.

Quinone Results

Mean particle-phase (PM_{2.5}) quinone/hydroquinone (Q-HQ) concentrations for cycles 1 and 2 are shown, respectively, in figures 5A and 5B. One interesting observation is that in Atascadero, while the levels of 1,2-NQ, 1,4-NQ, and PQ were comparatively much lower (figure 5A), the levels of AQ found in this rural agricultural area were remarkably similar to the levels found in urban San Dimas, and downwind in Riverside. While AQ concentrations (means from 0.110 to 0.134 ng m⁻³) did not vary much in Atascadero, San Dimas and Riverside (figure 5A), they ranged from 0.018 to 0.147 ng m⁻³ in Lompoc, Upland and Mira Loma (figure 5B). For the other Q-HQ, levels measured in late summer (cycle 2) were generally higher than during early summer (cycle 1).

In the urban sites of San Dimas and Riverside, during the early summer (cycle 1) the Q-HQ profiles are similar, suggesting common sources for these species (figure 5A), including direct vehicle emissions and formation during atmospheric transport. Levels of 1,2-NQ, 1,4-NQ, and PQ at these sites show a remarkable contrast with the low levels found in Atascadero. In the next report, we will fully evaluate seasonal and spatial differences for these 6 sites.

Carbonyl Results

Twelve carbonyls were measured in samples collected during cycles 1, 2 and 3. Although this limited carbonyl data set does not yet allow a full evaluation of seasonal/spatial trends, it is worth noting that similar carbonyl profiles were found at all sites.

For Atascadero, San Dimas and Riverside, the mean carbonyl concentrations were generally higher during the early summer period as compared with autumn (figures 6A-C), consistent with their photochemical production in the atmosphere. Levels found in rural Atascadero during the early summer and the autumn (figure 6-A) were generally lower than those in either San Dimas or Riverside (figures 6B-C).

The mean carbonyl levels measured during late summer (cycle 2) in Lompoc, Upland and Mira Loma, are shown in Figure 7. Levels measured at the urban sites of Upland and Mira Loma (cycle 2) are similar to levels measured in the early summer in San Dimas and Riverside (cycle 1). Carbonyl levels measured in the background site of Lompoc are comparable to the levels measured in Atascadero during the autumn period (cycle 3).

For all six sites reported (cycles 1, 2 and 3), four species, including formaldehyde, acetaldehyde, acetone and benzaldehyde accounted for 78-81% of the carbonyls measured. Further effects of seasonal and spatial variation on concentration will be available when the complete data set is available.

Conclusions

Although full sampler rotation has not been completed at the time of this report, we have observed both seasonal and spatial variations in the concentrations of the target species studied. When sampling is completed at these 6 sites, the annual levels of the respective pollutants at each location will be calculated and made available to CHS biostatisticians to evaluate possible association between chronic respiratory health outcomes and ambient air pollutant concentrations.

APPENDIX A

Table 1. PAH codes, molecular weight, subcooled liquid vapor pressure at 293 °K.

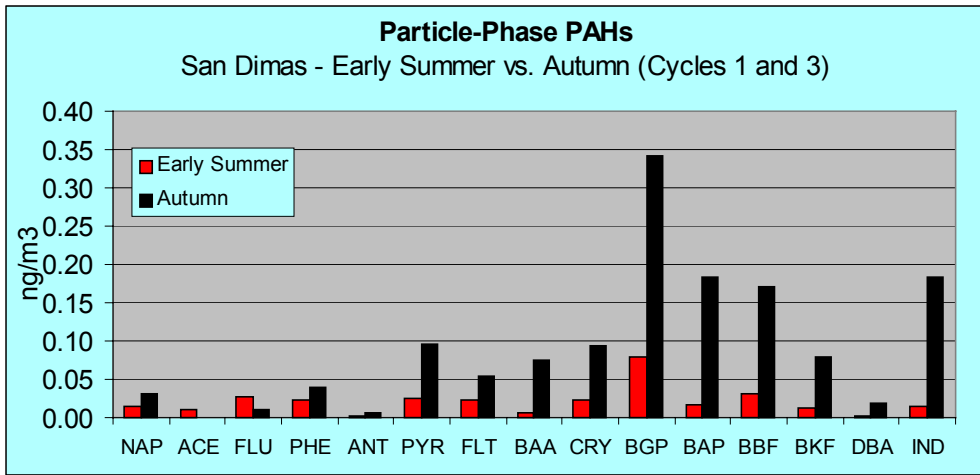
PAH	Code	MW	(log p ^o _L) ^a
naphthalene	NAP	128	1.59
acenaphthene	ACE	154	0.18
fluorene	FLU	166	-0.15
phenanthrene	PHE	178	-0.95
anthracene	ANT	178	-1.11
pyrene	PYR	202	-1.92
fluoranthene	FLT	202	-2.06
benzo(a)anthracene	BAA	228	-3.22
chrysene	CRY	228	-3.97
benzo(ghi)perylene	BGP	276	-4.65
benzo(a)pyrene	BAP	252	-4.67
benzo(b)fluoranthene	BBF	252	-4.99
benzo(k)fluoranthene	BKF	252	-5.39
indeno(1,2,3-cd)pyrene	IND	276	^b
dibenz(a,h)anthracene	DBA	278	-7.04

^aData from Peters et al, 2000, ^bNot available

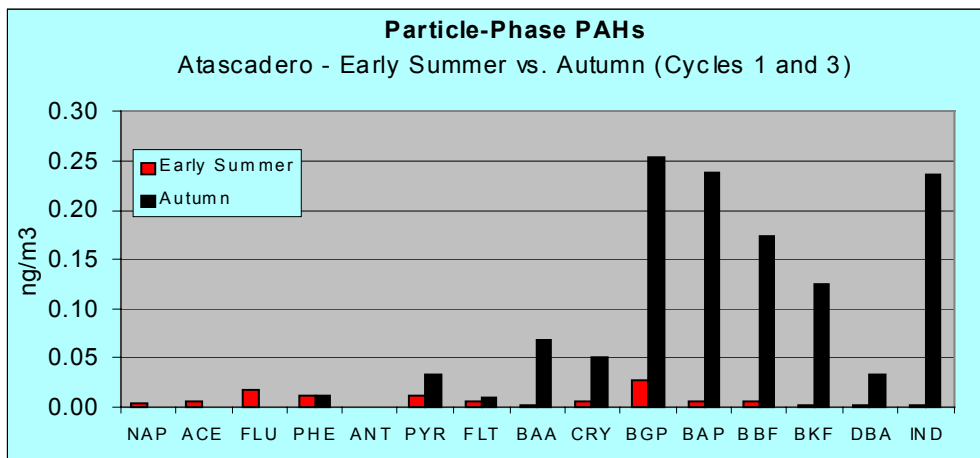
Table 2. Target Quinones and Carbonyls.

Code	Quinone
1,4NQ	1,4-naphthoquinone
1,2NQ	1,2-naphthoquinone
PQ	9,10-Phenanthrenequinone
AQ	9,10-Anthraquinone
Code	Carbonyl
FOR	formaldehyde
ACD	acetaldehyde
ACE	acetone
PRO	propionaldehyde
CRO	crotonaldehyde
BUT	butanone
MET	methachrolein
BUD	butyraldehyde
BEN	benzandehyde
VAL	valeraldehyde
MTO	m-tolualdehyde
HEX	hexaldehyde

A



B.



C

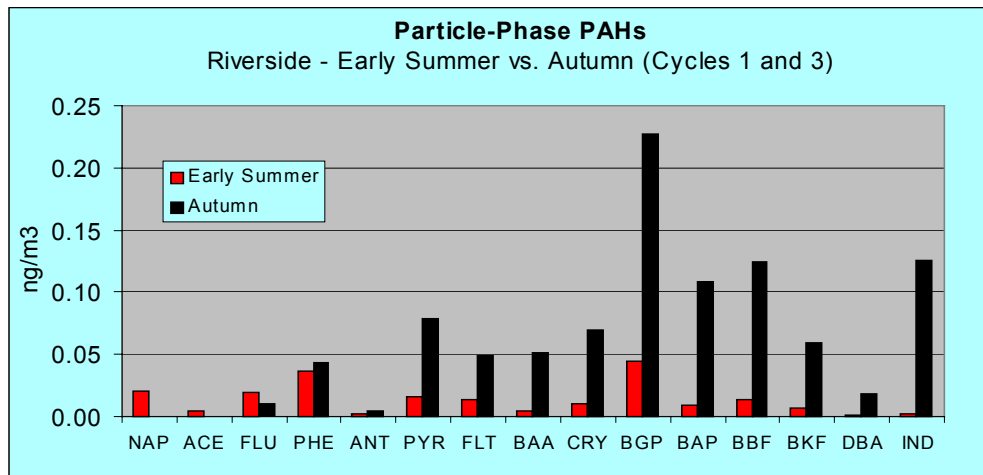
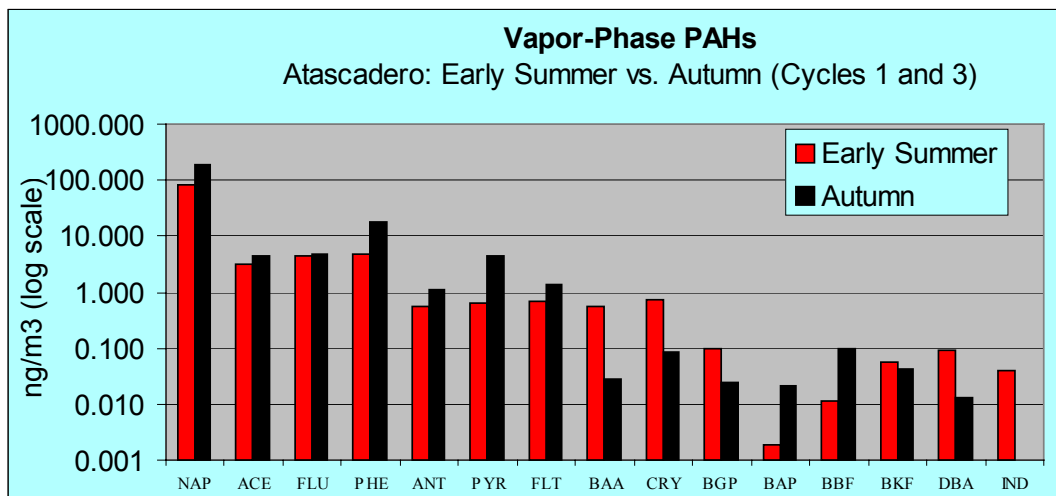
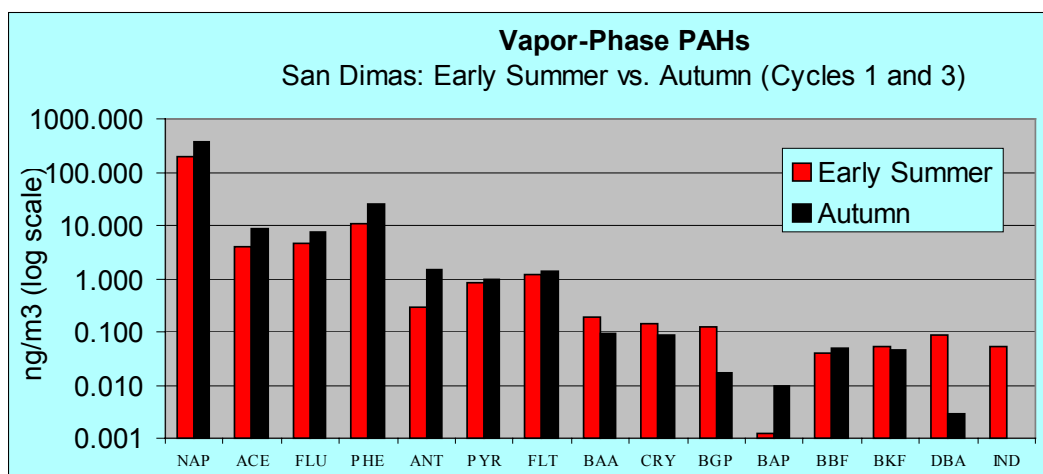


Figure 1. Comparison of mean particle-phase PAH concentrations between early summer (cycle 1, n=7,8,7) and autumn (cycle 3, n=8,8,8) for Atascadero (A), San Dimas (B) and Riverside (C).

A



B.



C

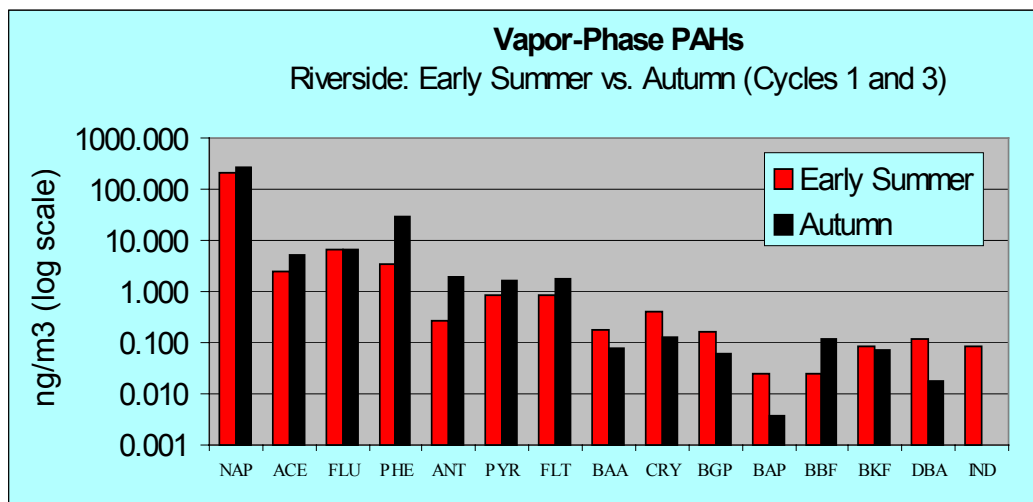


Figure 2. Comparison of mean vapor-phase PAH concentrations between early summer (cycle 1, n=7,8,7) and autumn (cycle 3, n=8,8,8) for Atascadero (A), San Dimas (B) and Riverside (C).

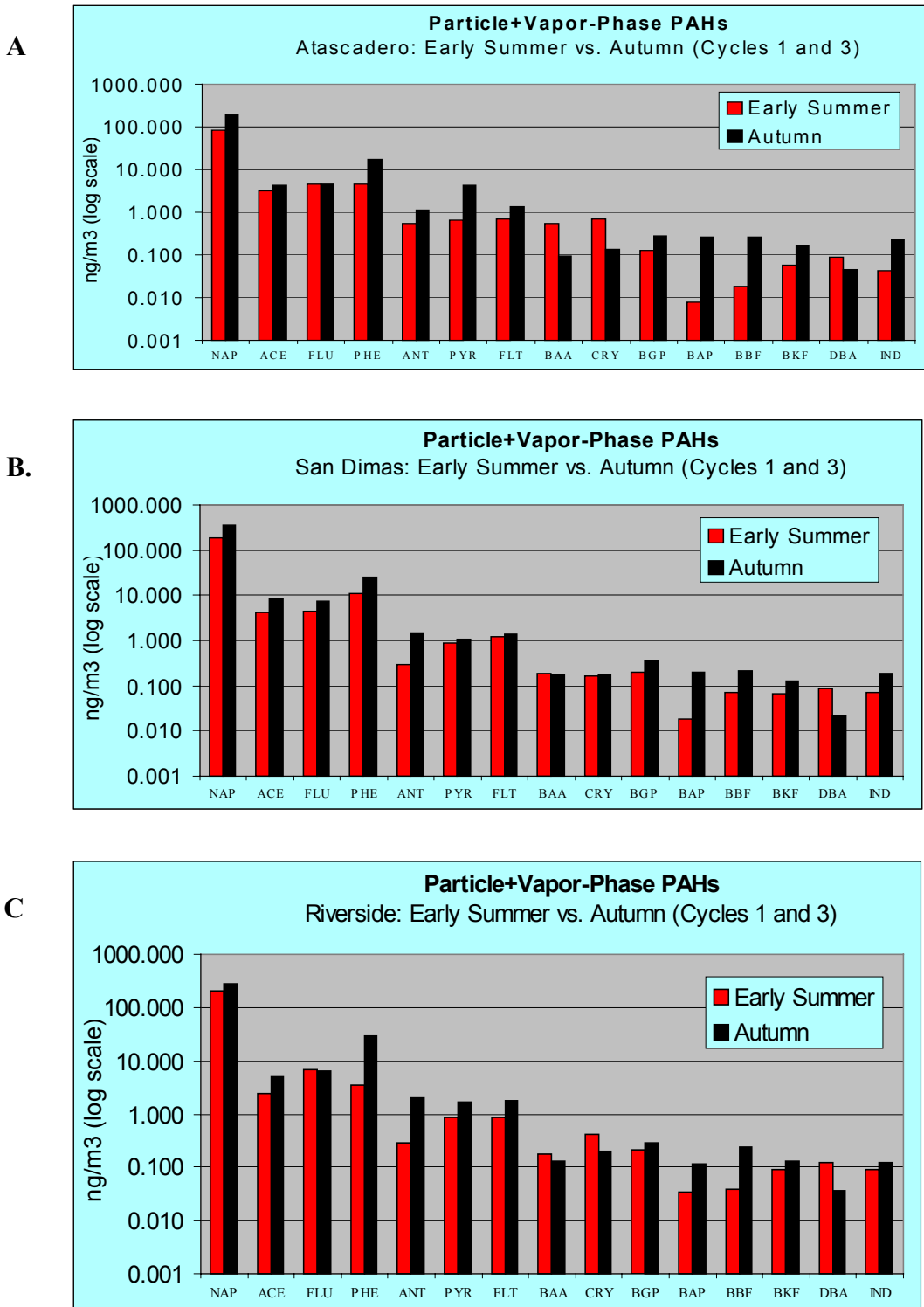
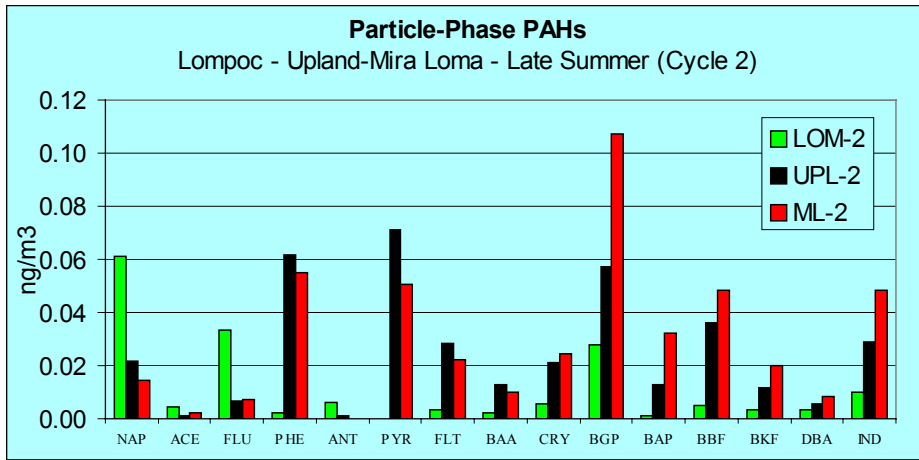
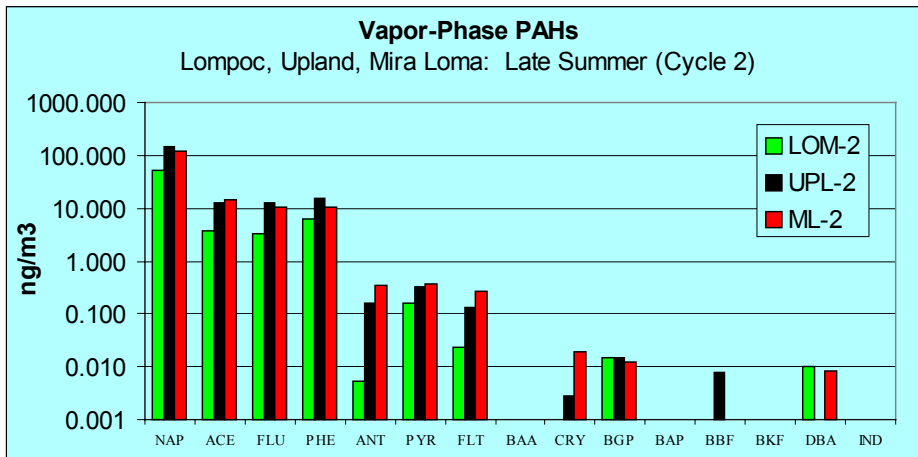


Figure 3. Comparison of mean total PAH concentrations between early summer (cycle 1, n=7,8,7) and autumn (cycle 3, n=8,8,8) for Atascadero (A), San Dimas (B) and Riverside (C).

A



B.



C

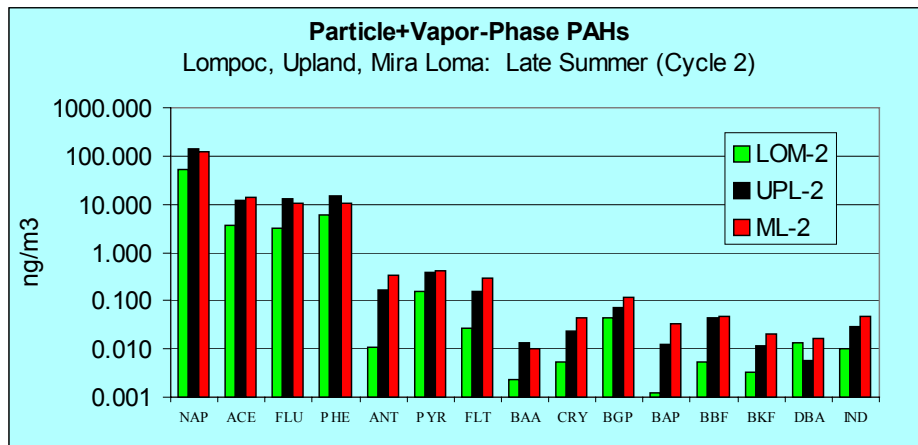
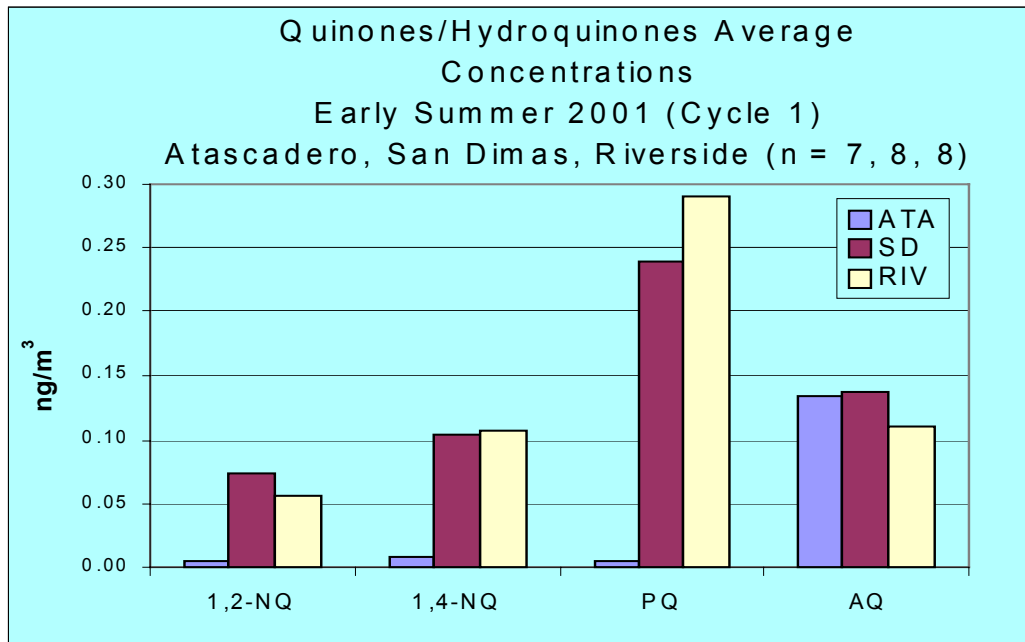


Figure 4. Mean PAH Concentrations for Cycle 2 (Late Summer, n=7,8,7) measured in the particle-phase (A), vapor-phase (B), and particle+vapor-phase (C) measured in Lompoc, Upland and Mira Loma.

A



B.

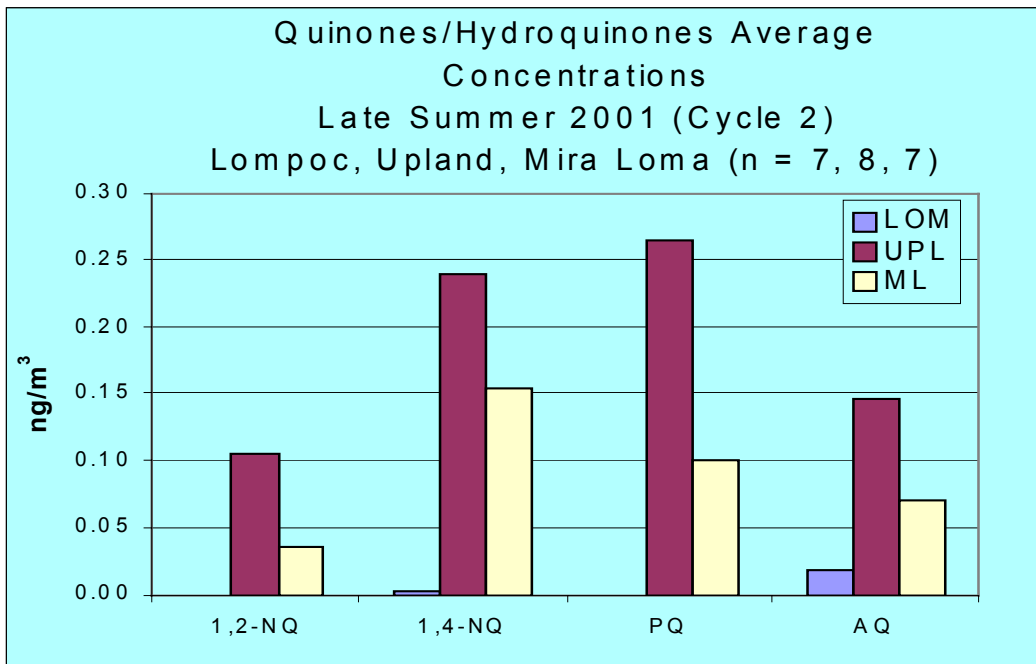
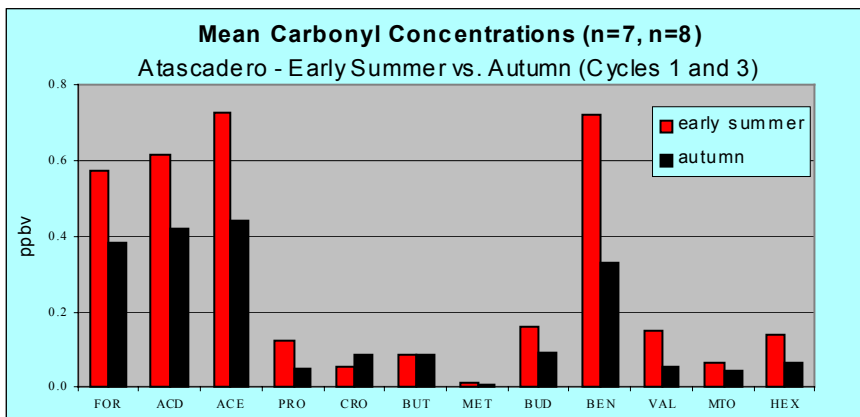
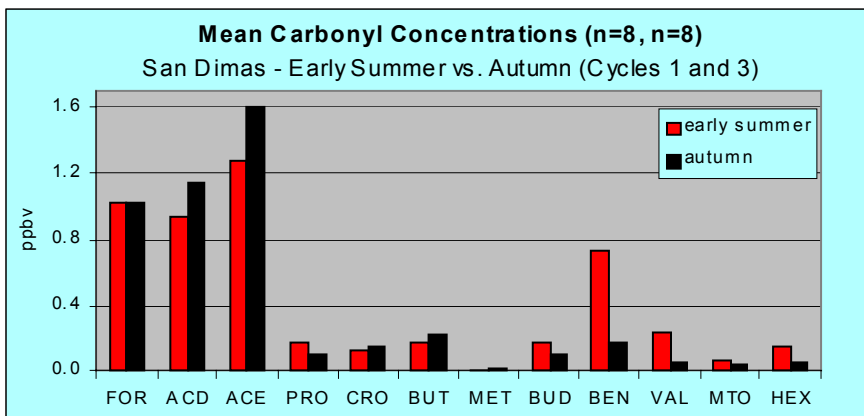


Figure 5. Mean particle-phase concentrations of quinones/hydroquinones for cycles 1 (A) and 2 (B).

A



B.



C

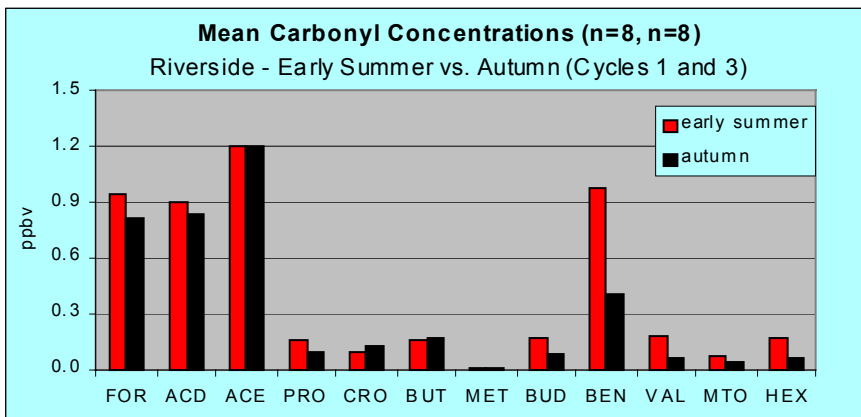


Figure 6. Comparison of mean carbonyl concentrations between early summer (cycle 1) and autumn (cycle 3) for Atascadero (A), San Dimas (B) and Riverside (C).

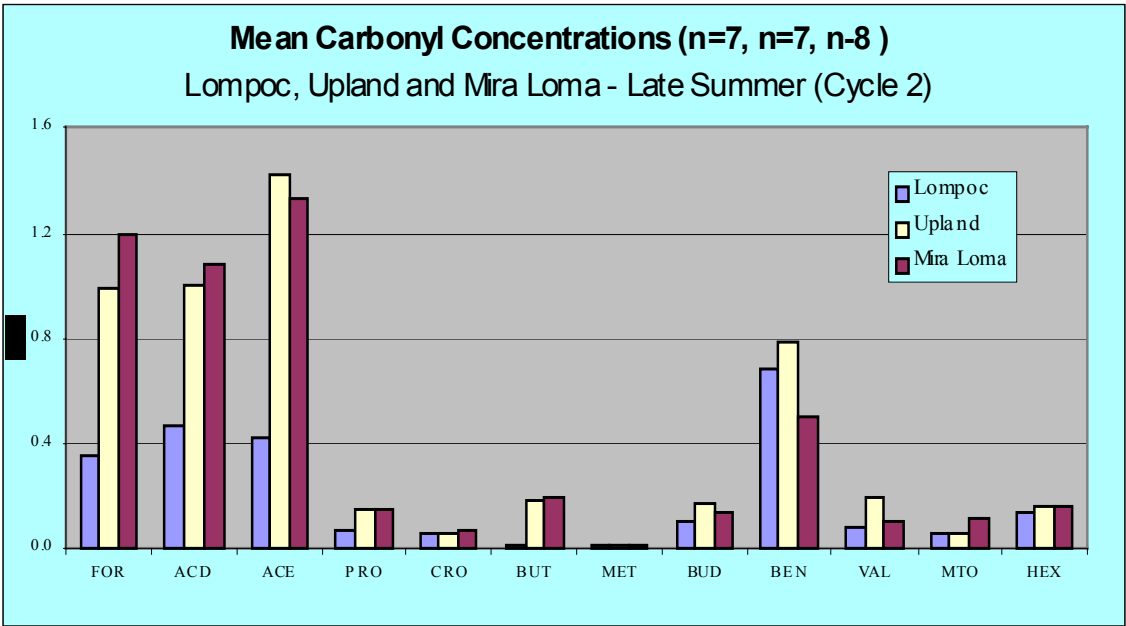


Figure 7. Mean carbonyl concentrations for cycle 2 (late summer) measured in Lompoc, Upland and Mira Loma

6. Automated, Size- and Time-Resolved Measurements of Particulate Carbon and Nitrate

Beginning in January 2002, we have simultaneous, size-resolved data on the concentration $PM_{2.5}$ nitrate and carbon at the Claremont site. Measurements are made for both species using our cascaded integrated collection and vaporization systems (ICVS). Nitrate is measured with a time resolution of 10 minutes in three size fractions:

<0.45 μm , 0.45-1.0 μm and 1.0-2.5 μm . Carbon is measured in the same three size fractions with 30-minute time resolution.

The collection method for both systems is the same. Each is comprised of three cascaded impaction and vaporization cells, as described earlier. The 2.5 μm cutpoint is provided by a single-jet impactor operated at ambient temperature and humidity. The particle sample stream is then denuded using an activated carbon honeycomb and equilibrated to a relative humidity of 65% before entering the cascaded collection cells. Thus, the particle size cuts at 0.45 μm and 1.0 μm corresponds to the denuded particle size at 65% RH and ambient temperature. Prior to entering the final stage the sample stream is humidified to above 90% RH in order to provide the most efficient collection.

For carbon, the sample is collected on a platinum substrate and is analyzed by flash-heating in a CO_2 free air stream. Evolved vapors pass over a bed of manganese dioxide heated to 650°C and are quantified by nondispersive infrared spectroscopy (LiCor LI-6252). Calibrations are done using aqueous standards of oxalic acid. Nitrate analysis is done by flash-vaporization in a nitrogen carrier gas with quantification of the evolved nitrogen oxides using a molybdenum catalyst-equipped chemiluminescence analyzer (TEI 42C).

Nitrate and carbon size distributions are compared in Figure 1 for from February 6 – 11, and in Figure 2 for February 18 – 26, 2002. For these subsets of data, and indeed throughout the measurement period to date, we find that the carbon and nitrate concentration profiles are very similar for the smallest size fraction. This size fraction, corresponding to particles below 0.45 μm in diameter, is generally associated with primary emissions or secondary compounds formed by gas-phase reactions with subsequent condensation on the preexisting aerosol.

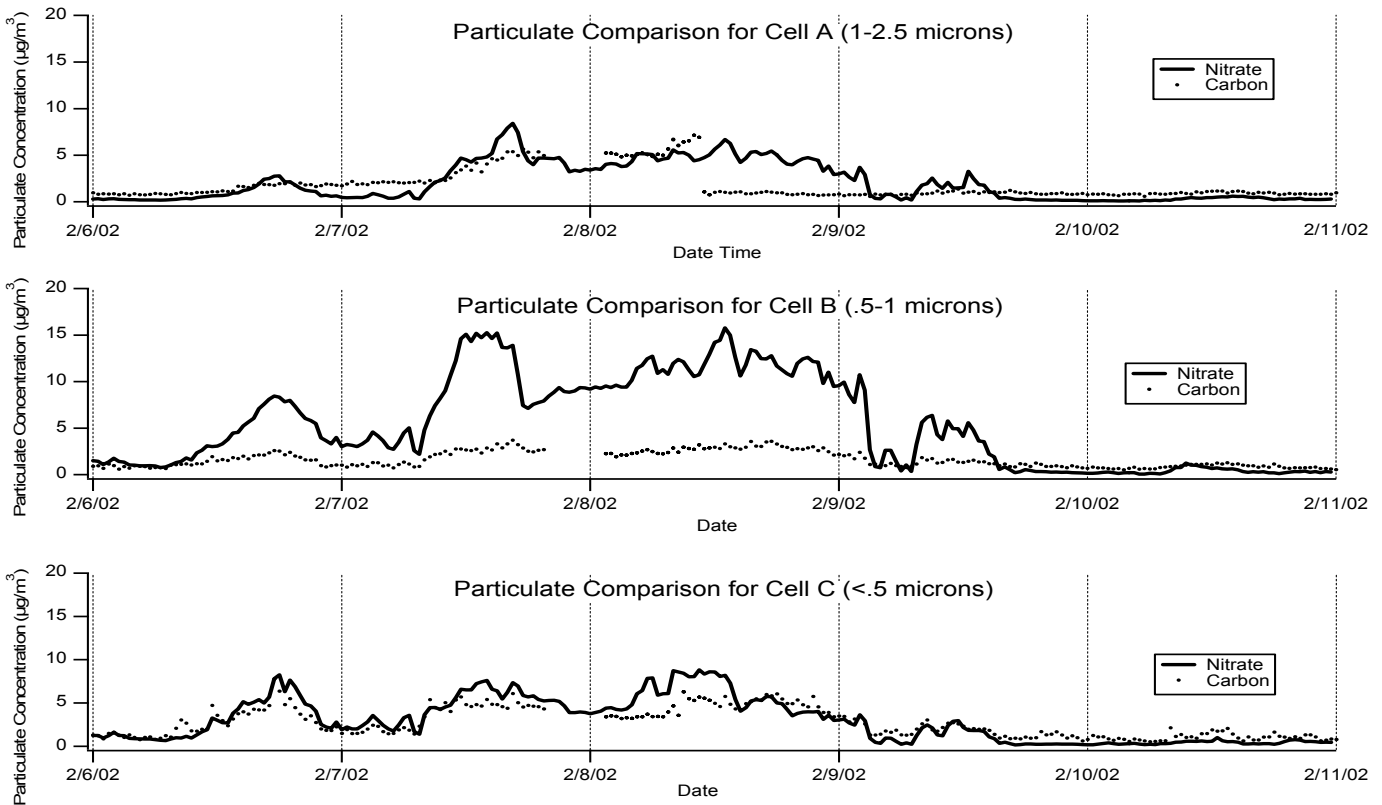


Figure 1. Comparison of ICVS particulate nitrate and carbon by size fraction at Claremont site.

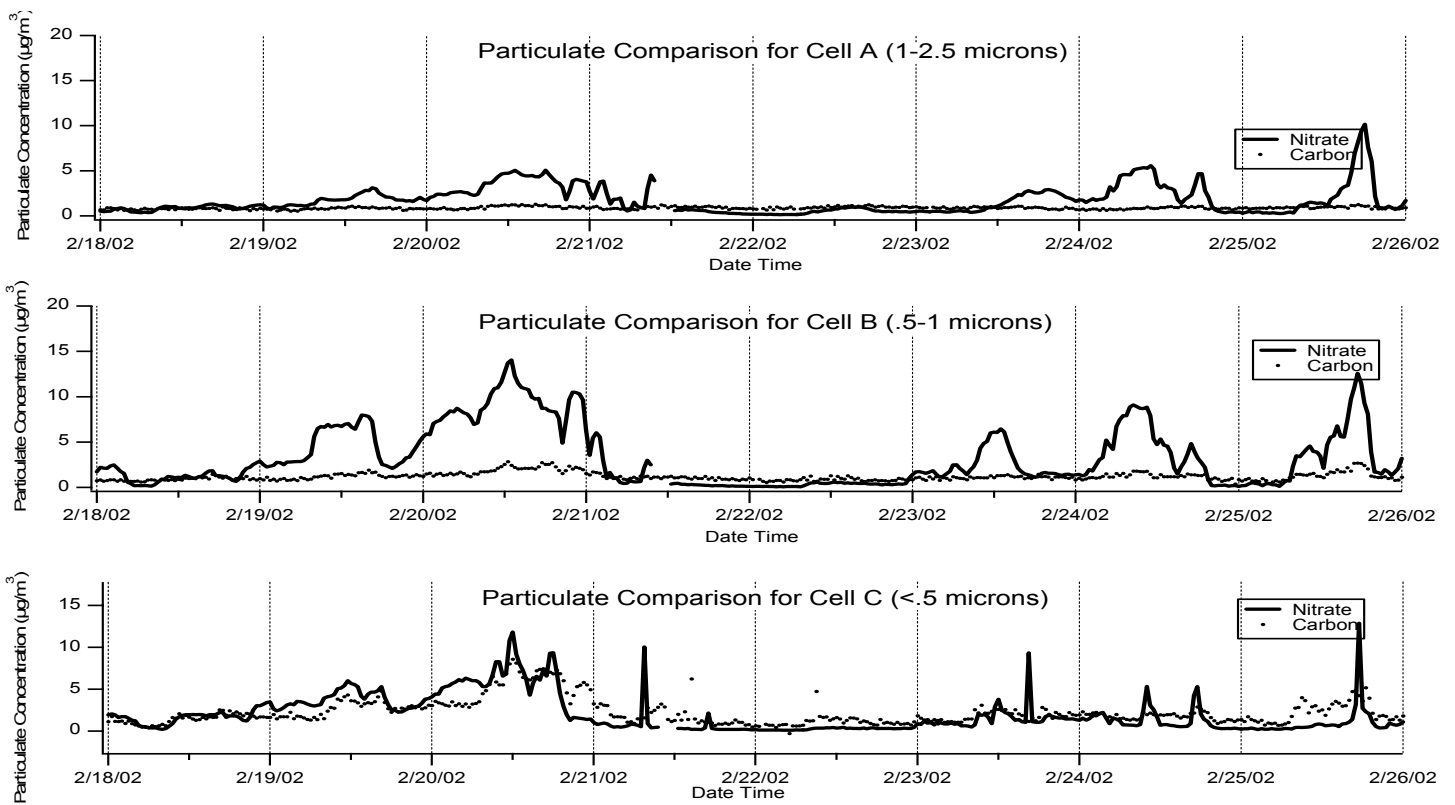


Figure 2. Comparison of ICVS particulate nitrate and carbon by size fraction at Claremont site.

Unlike the carbon, the nitrate aerosol concentrations often show a rapid increase at midday. This increase in nitrate is mostly associated with the “droplet mode” from 0.5 to 1 μm , with a corresponding smaller increase in the concentration from 1 to 2.5 μm (condensation mode). For sulfates, the dominance of the droplet mode is associated with heterogeneous formation processes. For nitrates, the dominance of the droplet mode indicates that particulate nitrate formation is dominated by the rate of uptake of nitric acid, or nitrate precursors, by the particles. If particulate nitrate formation were simply controlled by the rate of transport of nitric acid to the particle surface, this would lead to a size distribution that mimicked the condensation mode of the size distribution. This is not observed. Thus we must assume that the rate-limiting step is in the particle phase, and could be related to a size-dependent hygroscopicity of the aerosol. In contrast, the size distribution for carbonaceous aerosol is dominated by the condensation mode, and is consistent with the dominance of primary emissions from combustion or with homogeneous formation of secondary organics with subsequent condensation.

Figure 3 shows the difference in the time-variability between particulate nitrate and carbon, both in concentration and in mass mean diameters. Nitrate shows large midday peaks, whereas carbon is fairly flat, except for a slow increase the afternoon of February 20th. The carbon profiles may be the result of the combination of a primary source early in the day with secondary formation in the afternoons. Throughout the period, the mass mean diameter of the nitrates are consistently larger than for carbon.

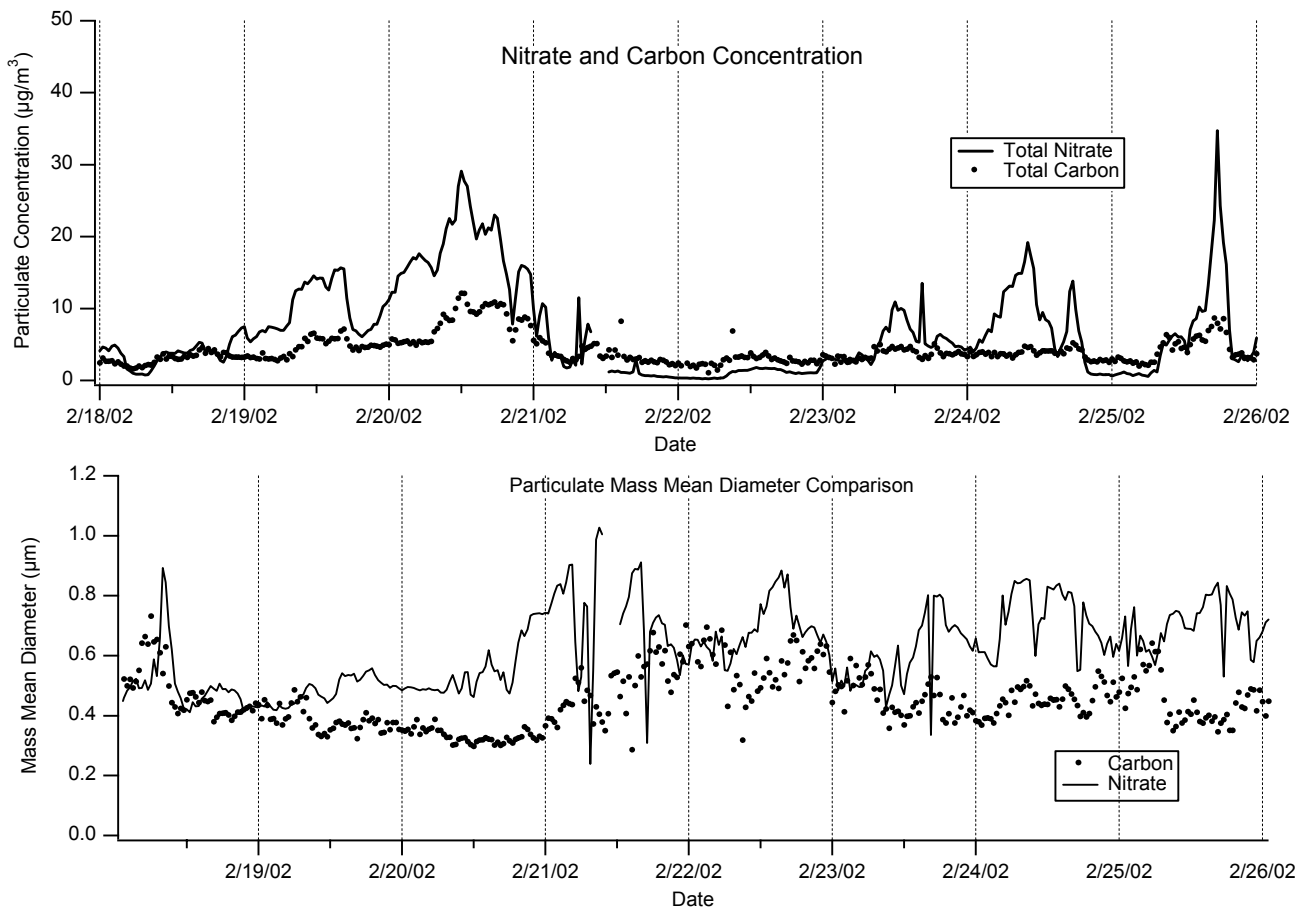


Figure 3. Comparisons of ICVS particulate nitrate and carbon total concentration, and particle mass mean diameter at Claremont site.

During this period at the Claremont site, Rupprecht and Patashnick operated a tapered element oscillating microbalance (TEOM) equipped with a dryer and an electrostatic precipitator. The electrostatic precipitator was turned on and off every five minutes, such that the TEOM alternately measured the mass change on the filter with, and without, particle collection. Without particle collection the filter was often observed to lose mass due to vaporization losses of already deposited material. PM_{2.5} mass is determined as the difference in the mass change on the filter with, and without, particle collection. Figure 4 compares the PM_{2.5} mass measurement and the magnitude of the loss correction, to the nitrate profile for the period from February 6 – 9, 2002. Here the nitrate values are scaled by a multiplier of 1.29 such that the nitrate is shown as the ammonium nitrate equivalent mass. Both the nitrate and the PM_{2.5} mass show the same detail in the time variability of the aerosol concentration. For example both data sets show local maxima on February 6th at 1800 and 1920, on Feb 7th at 0310, 0640, 1640 and 2110-2120. The magnitudes of the filter vaporization losses track the nitrate concentrations, with a delay of 1 to 2 hours. This data set provides a unique and valuable data set for evaluation of the kinetics of nitrate volatilization losses from filters.

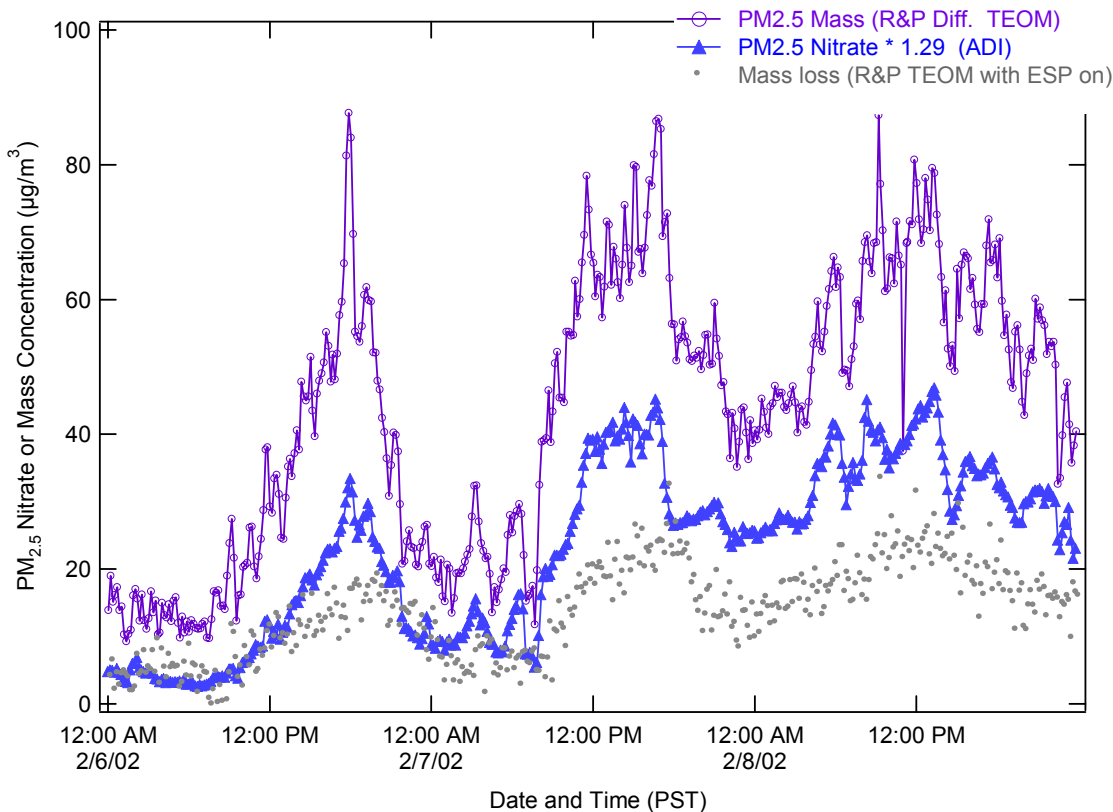


Figure 4. Comparison of ADI nitrate, expressed as equivalent ammonium nitrate mass, to PM_{2.5} mass and evaporative mass loss measured by a differential TEOM operated at 35C. The TEOM is equipped with an electrostatic precipitator that allows determination of, and correction for, the rate of evaporative losses from the collection filter.

7. Characterization of PAH and PAH-Derivatives

Background

The goal of our work is to characterize the polycyclic aromatic hydrocarbons (PAHs) and PAH-derivatives present at sites chosen to represent source sites or downwind receptor sites and to investigate the atmospheric chemistry occurring at these sites during different seasons. Of particular interest are nitro-PAH and nitro-polycyclic aromatic compounds (nitro-PAC) since these compounds are potent mutagens and have been observed as products of gas-phase atmospheric reactions of PAHs.

Nitro-PAC, including nitrated polycyclic aromatic ketones, have been found to be mutagenic in human cell and bacterial systems and should be viewed as potentially carcinogenic. 3-Nitrobenzanthrone (3NB), a powerful bacterial mutagen, was first identified by investigators using bioassay-directed fractionation of diesel emission particle extracts (Enya et al., ES&T, vol. 31, p 2772, 1997). Our laboratory demonstrated that 3NB is genotoxic using two human B-lymphoblastoid cell lines, MCL-5 and h1A1v2 (Phousongphouang et al., Mutation Research, vol. 472, p. 93, 2000). These results indicated that 3NB is an effective human cell mutagen, significantly inducing mutations at the tk and hprt loci in both cell lines, and inducing micronuclei in the h1A1v2 cell line.

It has been suggested that 3NB is formed in the atmosphere (Enya et al., 1998) as well as emitted from sources such as diesel exhaust. We decided, therefore, to conduct OH radical-initiated and NO₃ radical-initiated reactions of benzanthrene in the laboratory and investigate the nitrated products formed. We also undertook to analyze a diesel exhaust sample (NIST SRM 1975) and an archived ambient sample from Concord, CA for nitrobenzanthrones. The Concord, CA sample was chosen because it contains high levels of 2-nitrofluoranthene and 2-nitropyrene, nitro-PAH that have been shown to be formed from atmospheric reactions.

Experimental

Solution Phase Synthesis of Nitrobenzanthrones

3NB was synthesized by reacting ~550 mg of Bz with N₂O₄ in a 1:15 stoichiometric ratio in 150ml CH₂Cl₂ at room temperature. A drop of methanesulfonic acid was added to the mixture to catalyze the reaction. This reaction formed 3NB as the major mono-NB (MNB) isomer, along with one minor MNB isomer and several di-NBA (DNB) isomers. 3NB was separated from the MNB and DNB isomers by flash chromatography, and the fractions collected were analyzed by gas chromatography with mass spectrometry (GC-MS). The fraction containing the desired 3NB was then further purified by recrystallization and as quantified by GC with flame ionization detection (GC-FID) was >99% pure. 3NB was conclusively identified by HH-COSY and ¹H-NMR which were in general agreement with a previously reported spectra (Enya et al., ES&T, vol. 31, p 2772,, 1997).

2NB was synthesized by reacting ~200 mg Bz with N₂O₅ in a 1:4 stoichiometric ratio in 200ml CCl₄ at room temperature. This reaction formed 2NB as the major MNB isomer, along with another minor MNB isomer and several DNB isomers. 2NB was separated and purified as described for 3NB and as quantified by GC-FID was >99% pure. 2NB was also conclusively

identified by HH-COSY and $^1\text{H-NMR}$, again in general agreement with a previously reported spectra (Suzuki et al., Synthesis, p. 1273, 1997).

Atmospheric Reactions of Benzanthrone Producing Nitrobenzanthrones

The NB isomers were formed in the gas phase in a 7000-L all-Teflon atmospheric simulation chamber (ITC) by reaction of the parent compound, Bz, with the hydroxyl (OH) radical and with the nitrate (NO_3) radical. The ITC is equipped with blacklamps for irradiation, a Teflon-coated fan for mixing, and Pyrex sampling ports for reactant introduction and product collection. The reactions were performed at 298 ± 2 K and 740 Torr total pressure of purified air at ~5% relative humidity. Bz (~35 mg) was dissolved in 100 ml MeOH and introduced into the chamber by flowing high-purity nitrogen gas through a nebulizer with the ITC mixing fan on. After an additional 10-min of mixing, the radical-initiated reactions were conducted and the products were collected by sampling the chamber volume onto a polyurethane foam plug which was extracted and analyzed for nitrated products.

OH radicals were generated by the photolysis of methyl nitrite (CH_3ONO) and NO was also added to the reactant mixture to suppress the formation of ozone and, hence, of nitrate radicals. The initial reactant concentrations were 10 ppm each of CH_3ONO and NO, and the irradiation was carried out for 10 min. NO_3 radicals were generated by the thermal decomposition of N_2O_5 and NO_2 was also added to the reaction chamber. Initial reactant concentrations were 4 and 2 ppm of N_2O_5 and NO_2 , respectively. After a 10-min time period, allowing time for the reaction to occur but minimizing partitioning of the products to the walls, the reaction products were collected.

Approximately 90% of the chamber volumes were collected onto precleaned polyurethane foam (PUF) plugs placed in a Pyrex tube and connected directly to a high powered vacuum. The PUF plug from each reaction was Soxhlet extracted overnight in 100% CH_2Cl_2 . A 10ml aliquot was then precleaned by passing it through a silica gel column eluted with CH_2Cl_2 before analysis by GC-MS.

Identification of Nitrobenzanthrones in Ambient Particulate and Diesel Exhaust Extracts

Ambient Particle Extract. An aliquot of an ambient air particulate sample, previously collected, extracted, and stored in a freezer at -25°C , was analyzed for the presence of 2NB and 3NB. This particular sample was collected at an industrial emissions-impacted site in Concord, CA during December 1986 and January 1987 on high-volume filters. The sample extract was precleaned by open-column silica chromatography with 100% CH_2Cl_2 followed by 100% MeOH. The CH_2Cl_2 fraction was collected and concentrated by Rotavap for further HPLC fractionation on a Phase Sep (Norwalk, CT) normal-phase column (25 cm x 1 cm). The solvent program (at a flow rate of 3 ml min^{-1}) was as follows: initially 100% hexane for 10 min, followed by a 5-min gradient to 95% hexane and 5% CH_2Cl_2 . The solvent was programmed over the next 25 min to 100% CH_2Cl_2 , where it was held for 10 min; then programmed to 100% ACN over 10 min, held isocratic for 10 min; and then programmed back to the initial conditions. Beginning after 1 min, seven 9-min fractions of increasing polarity were collected for further preparation.

Of the seven fractions collected, fraction 4 was concentrated for analysis of nitro-PAH with molecular weight 247, i.e., the nitrofluoranthene (NF) and nitropyrene (NP) isomers.

Fractions 5 and 6, which were previously determined to be those in which Bz and the NB isomers would elute, were combined, concentrated, and further fractionated on a Vydac (Hesperia, CA) reverse-phase C18 column (25 cm x 1 cm). The solvent program employed for this further fractionation was 60% ACN and 40% H₂O held isocratic for 20 min at a flow rate of 3 ml min⁻¹. Three fractions were collected as follows: (RP1) 1-15 min, (RP2) 15-17 min, and (RP3) 17-20 min. RP2, which contained Bz and the NB, was then concentrated down to H₂O and then solvent exchanged into CH₂Cl₂ for GC-MS analysis.

Diesel Particulate Extract. Standard Reference Material (SRM) 1975, a diesel particulate extract, was obtained from the National Institute for Standards & Technology (NIST) (Gaithersburg, MD). The particulate sample was collected from diesel-powered industrial forklifts. The contents of one ampoule (~1.2ml) of extract was transferred to a 2 ml volumetric flask. The sample was spiked with an internal standard of 1-nitropyrene-d₉ (1NP-d₉) at an amount comparable to the concentration of 1-nitropyrene in the sample, based on measurements made at NIST and the volume was then brought up to 2 ml with CH₂Cl₂. Of the 2ml, 10% or 200 μl was processed for GC-MS analysis as described above, utilizing HPLC fractionation on the normal phase column followed by further fractionation on the reverse phase column.

GC-MS analyses for the nitro-PAC were performed on a 50m DB-17 capillary column (0.25mm i.d. and 0.25μm film thickness) using an HP5890 Series II GC interfaced to an HP5971A MS detector in the cool on-column mode. The selected ion-monitoring mode was utilized to monitor the molecular ions and characteristic fragment ions of Bz (m/z 230, 202) and NB (m/z: 275, 245, 229, 217, 201, 200, 189). The initial column temperature was 40°C, then temperature programmed to 300°C at 20°C min⁻¹, and held for 15 min. Selected ion monitoring mode was also utilized to monitor the molecular ions and characteristic fragment ions for the analysis of NF and NP (m/z: 247, 217, 201, 200, 189) and 1NP-d₉ (m/z: 256, 226, 210, 208, 198). For this analysis the initial column temperature was 40°C, then temperature programmed to 200°C at 20°C min⁻¹, then to 300°C at 2°C min⁻¹, and held for 15 min.

Results and Discussion

Syntheses of Nitrobenzanthrones

In aprotic solution, N₂O₅ undergoes dissociation to NO₃ and NO₂, allowing nitration by way of a radical reaction mechanism. The N₂O₅ reaction in CCl₄ often produces isomer profiles similar to those formed in gas-phase atmospheric reactions with the nitrate radical. 2NB was the main isomer formed in this reaction, along with another minor MNB isomer and several DNB isomers. This suggests that radical-initiated reactions of Bz that may occur in the atmosphere would result in the formation of primarily 2NB.

Reaction of N₂O₄ in CH₂Cl₂ is believed to proceed via an electrophilic mechanism, resulting in nitro-PAC products similar to those observed in combustion emissions. The N₂O₄ nitration formed 3NB as the major MNB isomer, along with one minor MNB isomer and several DNB isomers.

Nitrobenzanthrones Formed by Simulated Atmospheric Reactions

Both the OH radical-initiated and NO₃ radical-initiated reaction of gas-phase benzantrone resulted in the formation of 2NB (in the NO₃ radical-initiated reaction, a trace of 3NB was also observed). This is consistent with 2NB being the product observed in the solution-phase reaction of Bz with N₂O₅ in CCl₄ solution.

Identification of Nitro-PAC in Ambient and Diesel Particulate Extracts

Shown in Figure 1 are GC-MS mass chromatograms for the molecular ion ($m/z = 247$) of the NFs and NPs. The upper trace showing their elution order is of a standard solution containing all eight possible isomers. The middle trace is the result of the analysis of the Diesel SRM 1975, showing that the isomers present are those formed in electrophilic nitration reactions of pyrene (1NP) and fluoranthene (3NF and a trace of 8NF). The higher abundance of 1NP is attributed to the higher reactivity of pyrene relative to fluoranthene toward electrophilic nitration. The lower trace shows the results of the ambient sample collected in Concord, CA. 2-Nitro-fluoranthene and 2NP dominate (trace amounts of 1NP were also present), suggesting the OH radical-initiated reaction of fluoranthene and pyrene, producing 2NF and 2NP, respectively, had occurred.

Shown in Figure 2 are GC-MS mass chromatograms for the molecular ion ($m/z = 275$) of the nitrobenzanthrones. Again in the ambient sample (lower trace) the nitro-PAC isomer produced by atmospheric radical-initiated reactions, 2NB, is dominant. In contrast, the diesel exhaust sample (middle trace) contains 3NB.

The estimated levels of the NF and NP isomers in the ambient sample are: 2NF, 520 pg/m³; 2NP, 69 pg/m³, 1NP, 13 pg/m³. The estimated levels of the NB isomers in the ambient sample are: 2NB, 15 pg/m³; 3NB 0.4 pg/m³. Thus, in the Concord, CA ambient sample the nitro-PAH and nitro-PAC present at highest levels are those formed in situ in the atmosphere. Since these radical-initiated reactions occur in the gas phase, the higher level of 2NF relative to 2NB is consistent with the higher volatility of fluoranthene relative to benzantrone. In conclusion, 2NB can now be included as an addition marker compound for atmospheric nitro-PAC formation.

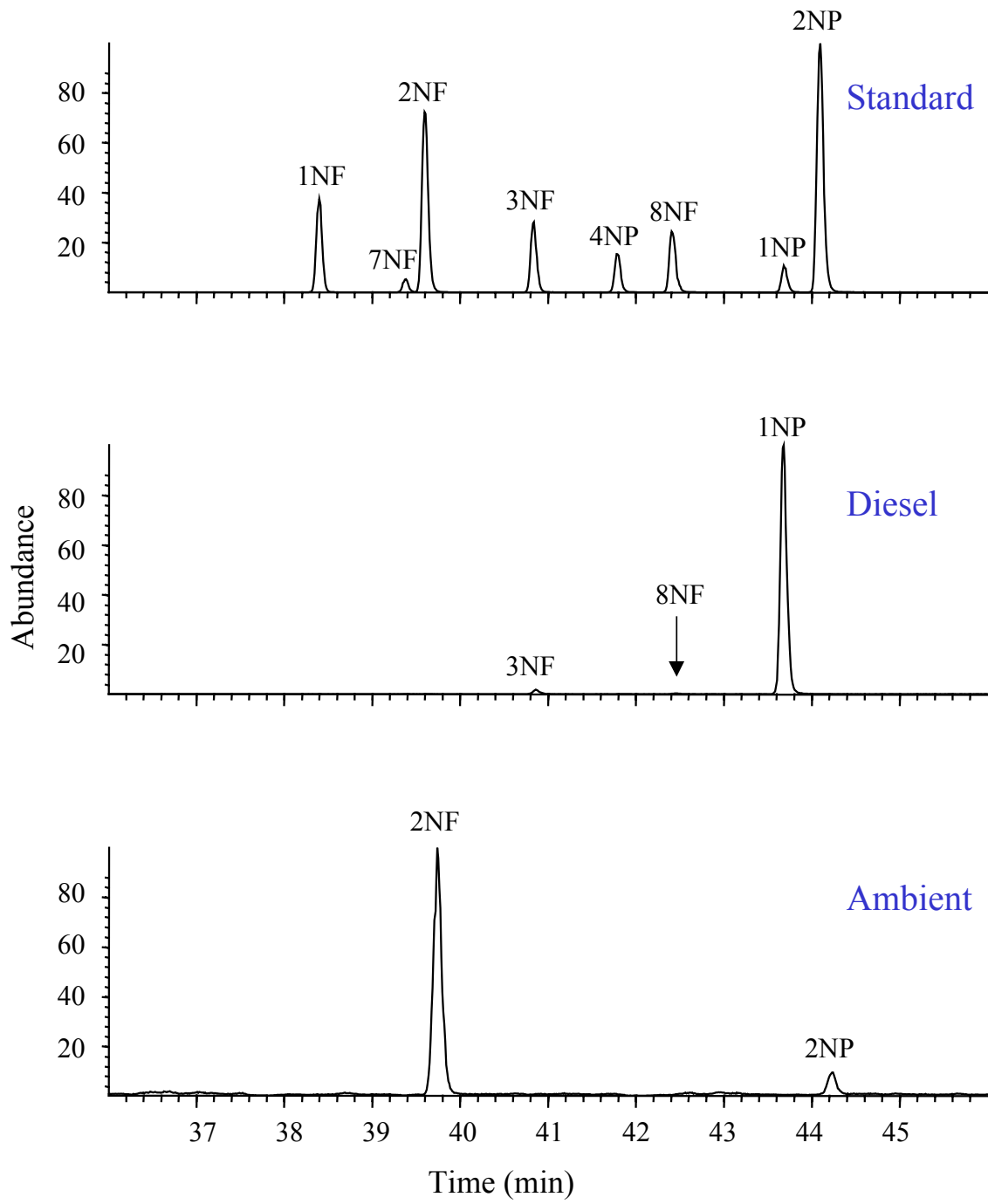


Figure 1.

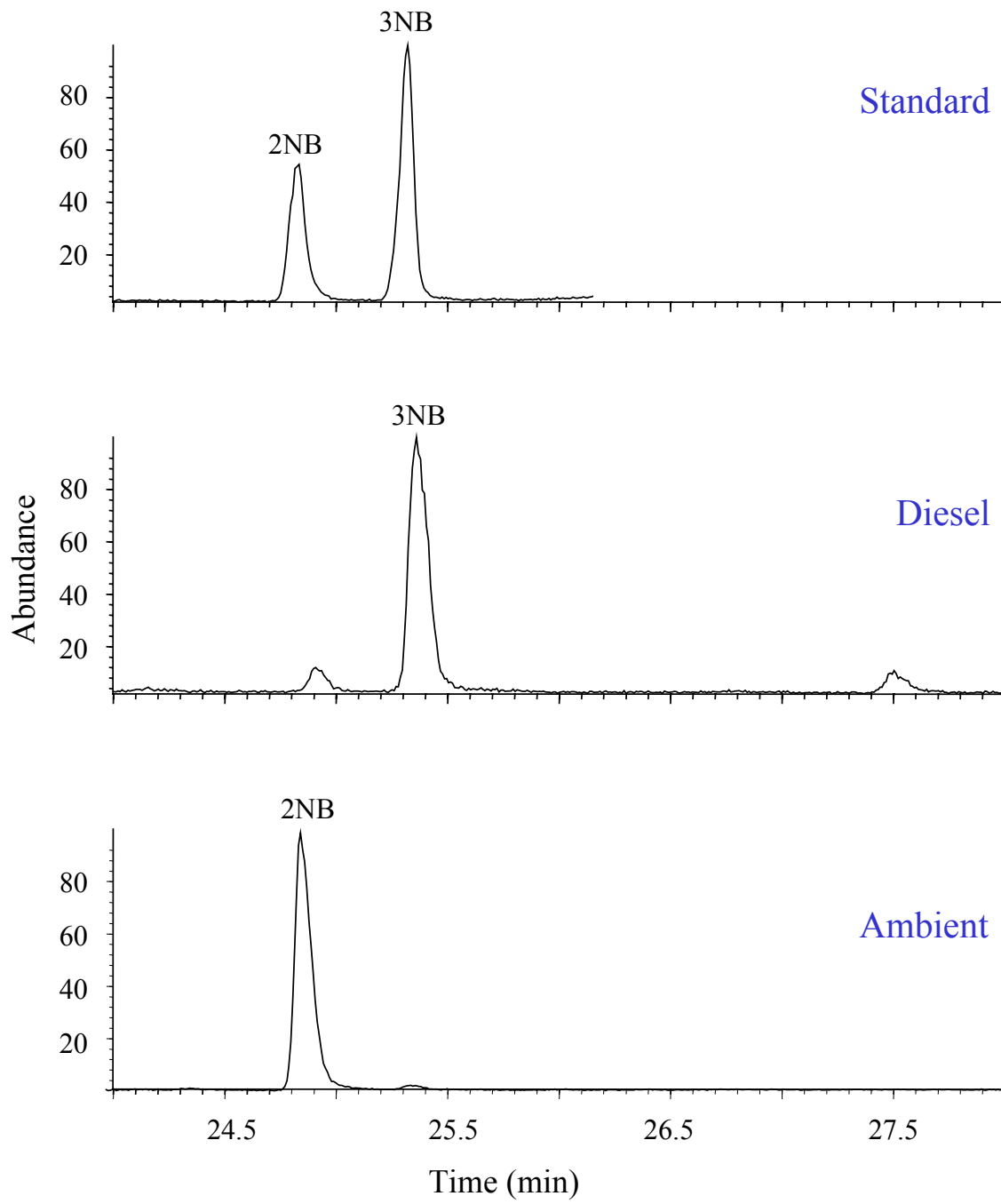


Figure 2.

8. Data Management of the Los Angeles Supersite

Summary

The major progress during this quarter was to clean up SMPS data collected from Downey, Riverside, and Rubidoux so that these data would be ready for submission to NARSTO. We regarded the raw SMPS data required great efforts to clean up for those were obviously outliers or potentially invalid data. Since there have been no criteria available in the literature to determine which were valid data and which were not, we have learned to develop some tentative criteria and attempted to apply uniformly among different data sets and assure these data were valid. We, in this progress report, briefly summarize what we have learned about SMPS data characteristics and some proposed criteria to clean up these data for quality control purposes. Given such unexpected difficulties, an updated submission schedule is also attached.

SMPS Data

SMPS data collected at these three sites by PIU include: Downey data from 09/22/2000 – 10/17/2000 (Downey – 0), 12/08/2000 – 12/10/2000 (Downey – 1), 12/13/2000 – 02/05/2001 (Downey – 2), Riverside data from 02/14/2001 – 06/05/2001 (Riverside), Rubidoux data from 06/25/2001 – 08/22/2001 (Rubidoux – 1), and 08/22/2001 – 09/08/2001 (Rubidoux – 2). Table 1 shows sampling date, number of channels set for sampling particles, particle size ranges, and number of records by date/time.

Q-Q Plots

We first used Q-Q plots to assess the overall behavior of each 15-min sampling record. The plot compares ordered values of log total concentration of particles for every 15 minutes with quantiles of a specified theoretical distribution such as the normal distribution. The rationale was that if the data distribution matches the theoretical distribution, although chosen empirically, the points on the plot form a linear pattern; and if not, unexpected data characteristics may have occurred. Our goals were to assess the pattern of abnormality and to find out which data records or even individual data values were obviously outliers or potentially invalid. Figures 1 – 6 depict Q-Q plots for log total concentrations from the 6 data sets listed in Table 1.

Examinations of these figures give an overall picture about general characteristics about each data set. First, all figures show data were clustered or scattered at certain regions. For example, four regions, from low to high concentrations, appear approximately in Figure 5. Data within each region seems to behave similarly, according to the lognormal assumption. If data behave relatively different from other peers, they are considered potentially invalid and require further investigations. For example, an extremely high-value outlier can be easily detected in Figure 2. Examination of this record showed SMPS generated a spike-like value in one of the 54 channels. Deletion of this spike value gave back the normal behavior of the remaining 53

values. Therefore, it is unwisely to delete the whole record, instead of deleting only one of the 54 values in this particular record.

During the past quarter, we made most our efforts to develop efficient criteria to screen out ‘good’ and ‘bad’ data. We have developed statistical and graphic techniques, such as the Q-Q plot shown in this report, to detect outliers, such as spikes with each record, and potentially invalid measurements. These methods are not detailed in this progress report and would be described in a research paper in the near future.

Submission of SMPS data to NARSTO

All these data described in Table 1 are in the final stage of quality check-up and will be delivered to NARSTO at the end of June. An updated submission is also attached in Table 2.

Table 1. SMPS data sets at Downey, Riverside, and Rubidoux

Data set	Sampling Dates	Particle Sizes (nm)	# of Channels	# of Records ^c
-----	-----	-----	-----	-----
Downey - 0	09/22/2000 - 10/17/2000	13.8 – 673.2	55	2196
Downey – 1	12/08/2000 – 12/10/2000	14.9 - 673	54 ^a	232
Downey – 2	12/13/2000 – 02/05/2001	14.1 - 661	108 ^b	3721
Riverside	02/14/2001 – 06/05/2001	14.1 - 661	108 ^b	9245
Rubidoux – 1	06/25/2001 – 08/22/2001	21.7 - 429	84	5160
Rubidoux –2	08/22/2001 – 09/08/2001	14.1 - 638	107 ^c	1278
-----	-----	-----	-----	-----

^aExclude one channel size with all values = 0. ^bExclude three channel size with all values = 0.

^cExclude four channel size with all values = 0. ^eA record is a series of variables, including particle concentration for a particular size, reported by SMPS for every 15 minutes.

Table 2. Status of LA Supersite Data Submitted to NARSTO

Status Date: 2002/06/14

Instrument	Type of Data		Data Submitted to NARSTO*	Data Accepted by NARSTO
	Location	Sampling Dates		
APS	Downey	12/08/00-02/05/01	01/24/2002	<u>04/09/2002</u>
	Riverside	02/14/01-06/05/01	03/08/2002	<u>04/09/2002</u>
	Rubidoux	06/25/01-08/26/01	03/08/2002	<u>04/09/2002</u>
SMPS	Downey	09/22/00-01/31/01	2Q/2002	
	Riverside	02/14/01-06/01/01	2Q/2002	
	Rubidoux	06/25/01-09/04/01	2Q/2002	
DataRAM	Downey	09/15/00-10/13/00	3Q/2002	
	Riverside	12/19/00-06/01/01	3Q/2002	
	Rubidoux	06/26/01-09/08/01	3Q/2002	
Partisol	Downey	11/15/00-02/02/01	3Q/2002	
	Riverside	02/05/01-05/25/01	3Q/2002	
	Rubidoux	06/27/01-08/29/01	3Q/2002	
TEOM	Downey	11/28/00-02/05/01	3Q/2002	
	Riverside	04/03/01-05/22/01	3Q/2002	
Automet	Downey	12/08/00-02/05/01	3Q/2002	
	Riverside	02/05/01-03/19/01	3Q/2002	
	Rubidoux	06/19/01-09/08/01	3Q/2002	
Aethalometer	Riverside	02/21/01-06/05/01	4Q/2002	
	Rubidoux	06/25/01-09/08/01	4Q/2002	
MetOne	Riverside	03/21/01-06/05/01	4Q/2002	
	Rubidoux	06/19/01-09/08/01	4Q/2002	
Nitrate	Rubidoux	07/18/01-09/02/01	4Q/2002	
Aethalometer		10/08/01-12/07/01	1Q/2003	
APS		09/17/01-11/22/01	1Q/2003	
Automet		09/17/01-11/01/01	1Q/2003	
Carbon		10/12/01-11/16/01	1Q/2003	
DataRAM	Claremont	10/08/01-12/07/01	1Q/2003	
MetOne		10/17/01-12/07/01	1Q/2003	
Nitrate		09/08/01-11/28/01	1Q/2003	
Partisol		10/15/01-11/28/01	1Q/2003	
SMPS		09/17/01-11/22/01	1Q/2003	

Q-Q Plot of Total Conc for All Data at Downey 0

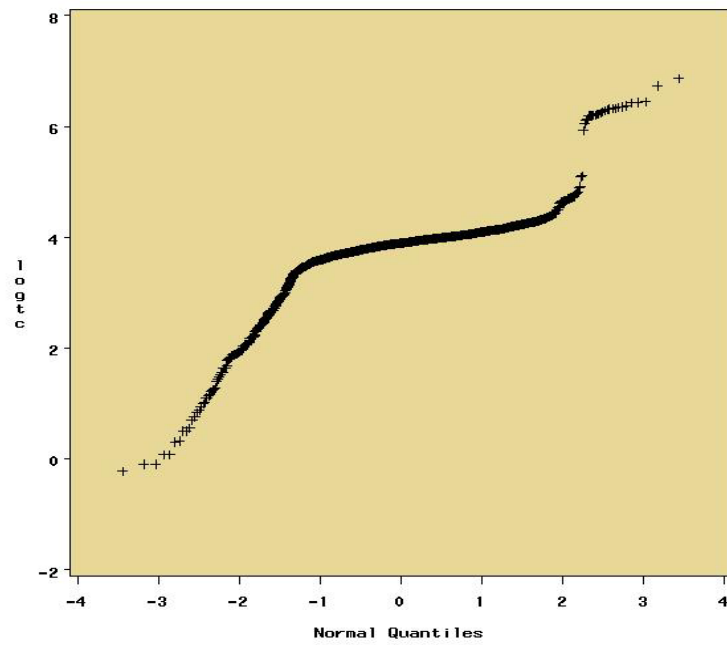


Figure 1.

Q-Q Plot of Total Conc for All Data at Downey 1

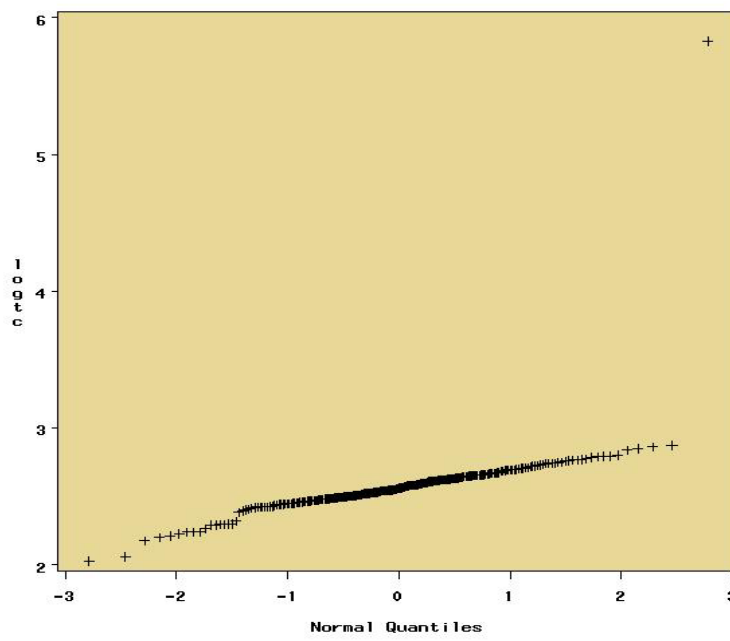


Figure 2.

Q-Q Plot of Total Conc for All Data at Downey 2

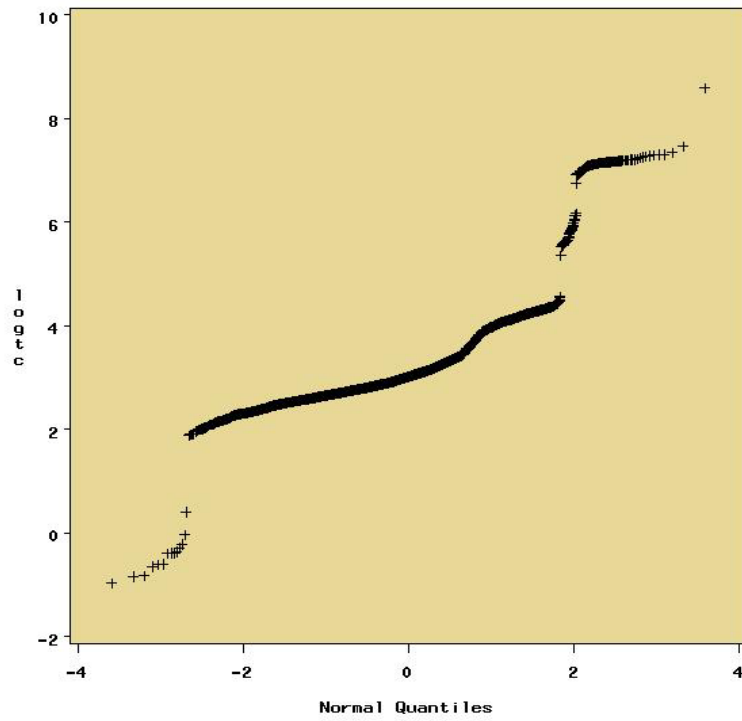


Figure 3.

Q—Q Plot of Total Conc for All Data at Riverside

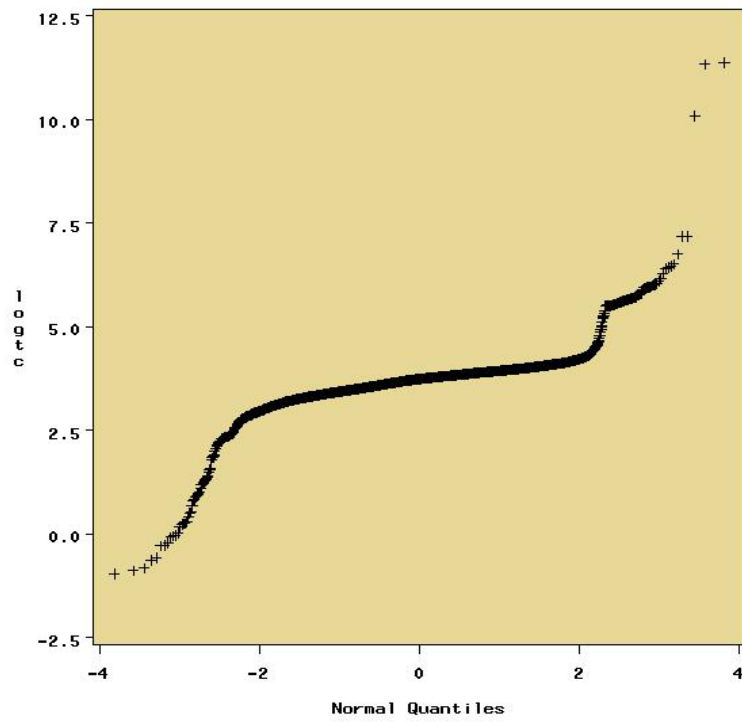


Figure 4.

Q—Q Plot of Total Conc for All Data at Rubidoux (1)

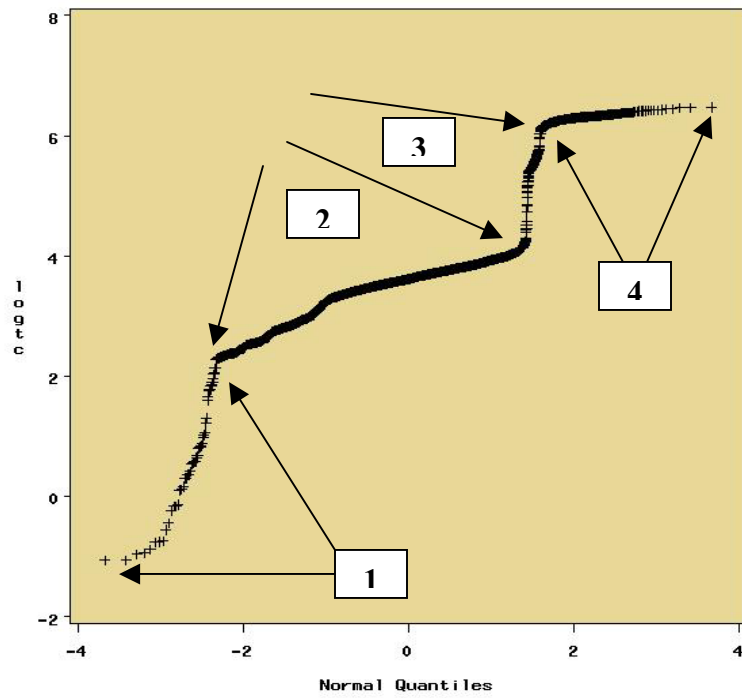


Figure 5.

Q—Q Plot of Total Conc for All Data at Rubidoux (2)

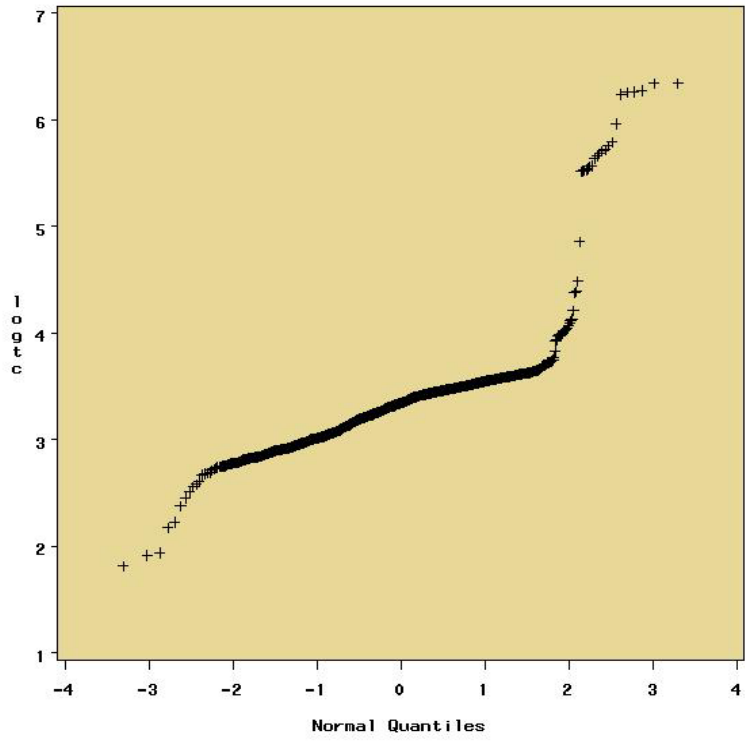


Figure 6.